LIGHT SENSING PROPERTY OF AMORPHOUS SILICON THIN FILM PIN DIODE: SOLAR CELL AND PHOTODIODE

A Dissertation

by

KIBUM KIM

Submitted to the Office of Graduate and Professional Studies of
Texas A&M University
in partial fulfillment of the requirements for the degree of

DOCTOR OF PHILOSOPHY

Chair of Committee,	Yue Kuo
Committee Members,	Zhengdong Cheng
	Philip R. Hemmer
	Jorge M. Seminario
Head of Department,	Ibrahim Karaman

May 2017

Major Subject: Materials Science and Engineering

ABSTRACT

The performance and stress-induced degradation of a-Si:H solar cells with pin and nip stacked structures prepared in the single chamber PECVD have been studied. The property of the i-layer depends on the sequence of film deposition because the intrinsic (i)-layer is contaminated by the dopant residue in the chamber remaining from the previous deposition step. This affects the solar cell performance, degradation, as well as recovery. Also, the cell degradation under the electric-stress condition with and without the simultaneous light exposure has been studied.

The light sensing characteristics of the a-Si:H pin diode composed of both top and bottom ITO electrodes with respect to the power density of red (625nm), green (530nm), and blue (470nm) illumination lights have been studied. The study's findings indicate that the light detection of the diode is affected by both the wavelength and power density of the incident light. Such influence turns out to be due to the dependence of the asymmetric carrier loss on the light wavelength and power density. Also, changes in pin diode characteristics have been confirmed by internal resistances, short circuit current density, and open circuit voltage, as well as the application of a bottom light reflector.

The mechanism of asymmetric carrier transfers in the light-sensing of the a-Si:H pin diode has been discussed using different i-layer thickness, combined electric-optical stress method, and three narrow-band lights. The position of the photo-generated electron-hole pairs within the i-layer varies with the wavelength of the incident light,

which directly affects the asymmetric transfer and loss of the carriers. This has been confirmed with the i-layer thickness and combined electric-optical stress method.

DEDICATION

This dissertation is gratefully dedicated to my beloved family: wife HyeGyeong Cho, father MinSeok Kim, mother MaengRye Park, and brothers KilDo Kim and MooKwon Kim.

ACKNOWLEDGEMENTS

I would like to sincerely thank my advisor, Dr. Yue Kuo, for his support and guidance on my research at Texas A&M University. During my Ph.D. time in Thin Film Nano and Microelectronics Research Laboratory, I have overcome plenty of obstacles and grown up mentally and academically. Also, I would like to thank my committee members, Dr. Zhengdong Cheng, Dr. Philip R. Hemmer, and Dr. Jorge M. Seminario. They have been very generous with their valuable time and suggestion.

For their support and technical discussion of my research, I thank my previous colleagues, Dr. Chi-Chou Lin, Dr. Geng-Wei Chang, I-Syuna Lee, Dr. Chur-Shyang Fuh, Dr. Dong Li, and Kai Henry. I am also thankful to my current colleague, Shumao Zhang, for the sputter deposition of metal electrodes used in this dissertation.

I am eternally grateful to my beloved family for all their support during my Ph.D. study. Without their sacrifices, I would never have completed my Ph.D.

CONTRIBUTORS AND FUNDING SOURCES

This work was supervised by a dissertation committee consisting of Professor Yue Kuo in the Department of Chemical Engineering and Materials Science and Engineering, Professor Zhengdong Cheng in the Department of Chemical Engineering and Materials Science and Engineering, Professor Jorge Seminario in the Department of Chemical Engineering and Materials Science and Engineering, and Professor Philip Hemmer in the Department of Electrical and Computer Engineering and Materials Science and Engineering

All metal electrode depositions for Chapter 3, 4, and 5 were provided by Sumao Zhang and all other work for the dissertation was completed independently by the author.

This work was made possible partially by NSF under 0968862.

TABLE OF CONTENTS

Page

ABSTRACT ii

DEDICATION iv

ACKNOWLEDGEMENTS v

CONTRIBUTORS AND FUNDING SOURCES vi

TABLE OF CONTENTS vii

LIST OF FIGURES ix

LIST OF TABLES xii

CHAPTER I INTRODUCTION 1

1.1 Overview 1
1.2 The photovoltaic effect 2
1.3 Hydrogenated amorphous silicon 3
1.4 p-n diode 13
1.5 pin diode 16
1.6 Outline of this dissertation 18

CHAPTER II EXPERIMENTAL 20

2.1 Plasma enhanced chemical vapor deposition 20
2.2 Optical and electrical property characterization 26

CHAPTER III INFLUENCE OF PIN AMORPHOUS SILICON STACK DEPOSITION SEQUENCE ON SOLAR CELL PERFORMANCE AND DEGRADATION 32

3.1 Introduction and motivation 32
3.2 Experimental 33
3.3 Influence of tri-layer deposition sequence on solar cell performance 34
3.4 Deterioration of solar cell under electric stress vs. electric-light combined stress 37

3.5 Degradations of a-Si:H solar cells of different tri-layer deposition sequences under electric-light combined stress condition……...…39
3.6 Recovery of degraded solar cell……...46
3.7 Summary……...……..……..48

CHAPTER IV WAVELENGTH AND POWER DENSITY EFFECTS ON LIGHT SENSING OF a-SI:H PIN DIODE……..……49

4.1 Introduction and motivation .....…49
4.2 Experimental 50
4.3 Wavelength effect on EQE…….……..52
4.4 Light intensity effect on EQE……...…54
4.5 Light wavelength and power intensity effects on diode characteristics……..….61
4.6 Back reflector effect…….…...…65
4.7 Summary…….……..…66

CHAPTER V MECHANISM OF ASYMMETRIC CARRIER TRANSFERS OF a-SI:H PIN DIODE...…….....68

5.1 Introduction and motivation 68
5.2 Experimental 69
5.3 Intrinsic layer thickness effect……..……..…..71
5.4 Carrier loss mechanism……...……..…74
5.5 Defect generation in intrinsic layer…….…..76
5.6 Thickness vs. defect density effect under red light illumination……..79
5.7 Summary…….……..80

CHAPTER VI CONCLUSIONS 81

REFERENCES 83

LIST OF FIGURES

Figure		Page
1	Overview of amorphous silicon thin film pin diode	2
2	Band diagram of the photovoltaic effect (filled circle: electrons and Empty circle: holes)	3
3	Atomic configurations of (a) crystalline silicon, (b) amorphous silicon, and (c) hydrogenated amorphous silicon	5
4	Atomic bonding models of (a) crystalline silicon, (b) amorphous silicon, and (c) hydrogenated amorphous silicon	7
5	Electronic density of states in a-Si:H	10
6	I-V characteristic of p-n junction	13
7	Formation of p-n junction in band diagram	15
8	Band diagram of p-n junction under (a) bias = 0V, (b) bias > 0V, and bias < 0V	16
9	Band diagram of (a) pin diode under open-loop condition and (b) light-illuminated pin diode and its carrier collection mechanism under closed-loop condition	18
10	Simplified PECVD reactor	24
11	ITO patterning process flow	25
12	Optical measurement setup	26
13	Current density (J) – voltage (V) characteristic of a-Si:H pin diode under light illumination condition	27
14	Shunt (R_{sh}) and series resistance (R_S) of a-Si:H pin diode under light illumination condition	31
15	Schematic structure of (a) pin ($p^+p^-n^+$) and (b) nip ($n^+n^-p^+$) structured solar cells	36

16 Stress time dependence of normalized efficiency ($p^+p^-n^+$ cell) on electric stress with and without light illumination……39

17 Variation of power conversion efficiency of solar cells with time under combined electric and light stress condition. Inset: power law dependence of PCE on stress time for $p^+p^-n^+$ cell……42

18 Changes of (a) J_{SC}, (b) V_{OC}, and (c) FF of $p^+p^-n^+$ and $n^+n^-p^+$ a-Si:H solar cells with time under combined current-illumination stress……...44

19 Changes of shunt and series resistances of (a) $n^+n^-p^+$ and (b) $p^+p^-n^+$ a-Si:H solar cells with time under combined electric-light (5V and AM 1.5G) stress……45

20 Changes of (a) V_{OC}, (b) J_{SC}, (c) FF, and (d) PCE of $p^+p^-n^+$ and $n^+n^-p^+$ a-Si:H solar cells with annealing time at 200℃. Devices was previously stressed for 60 hours under combined electric-light (5V and AM 1.5G) stress……...47

21 a-Si:H pin diode structure and experimental setup……51

22 EQE dependence on light wavelength and power intensity……...54

23 Changes of EQE with the illumination light power density of different lights…….……...56

24 Dependence of photo-current density on power densities of (a) red, (b) green, and (c) blue light illumination……...57

25 Light absorption of (a) n^+, (b) i/n^+, and (c) p^+in^+ layers of red, green, and blue incident lights at various power densities……60

26 I-V curves of a-Si:H pin diode under the illumination of (a) red, (b) green, and (c) blue lights at various light intensities……62

27 Changes of (a) R_S and (b) R_{sh} with the illumination light power density under red, green, and blue light illumination conditions……..……63

28 Relationship between short circuit current density (J_{SC}) and open circuit voltage (V_{OC}) of a-Si:H diode on the increase of light intensity……..64

29 Effect of Ag reflector on EQE at different light power densities of (a) red, (b) green, and (c) blue LED……..…….66

30 a-Si:H pin diode structure……..……70

31 J-V characteristics of the a-Si:H diode with (a) 300 and (b) 200 nm i-layer under red, green, and blue light illuminations…….....…72

32 Dependence of current density drop rate and EQE on red, green, and blue light illuminations……...…...73

33 Possible carrier loss mechanism of negative biased diodes with (a) 300 and (b) 200 nm thick i-layer under blue light illumination……....75

34 J-V characteristics of the same diode with 200 nm i-layer after (a) 0, (b) 5, and (c) 10 min of combined electric-light exposure stress……...……77

35 Changes of current density drop rate and EQE of the diode on combined stress under three different lights…….…..78

LIST OF TABLES

Table		Page
1	Deposition condition of pin or nip a-Si:H films…….…….....34	
2	Initial efficiency of $p^+p^-n^+$ and $n^+n^-p^+$ cells……...…35	
3	Deposition conditions of a-Si:H pin diode……..……52	
4	Deposition conditions of a-Si:H pin diode……..…71	

CHAPTER I

INTRODUCTION

1.1 Overview

Because hydrogenated amorphous silicon (a-Si:H) pin diode is effectual in harvesting broadband lights,[1] it has been used as solar cells or photodiodes.[2, 3] This fact indicates that that kind of device shares the same pin structure. The application of the pin diode is dependent on preferred functions. For example, the pin diode behaves like a solar cell when exposed to broad band solar light, whereas it plays like a photodiode when exposed to narrow-band lights with diverse intensities. The light-harvesting function of the a-Si:H diode was delivered by the following three important discoveries: the photovoltaic effect, p-n diode, and amorphous silicon. This introduction presents these fundamentals. Figure 1 summarizes the overview of the a-Si:H pin diode.

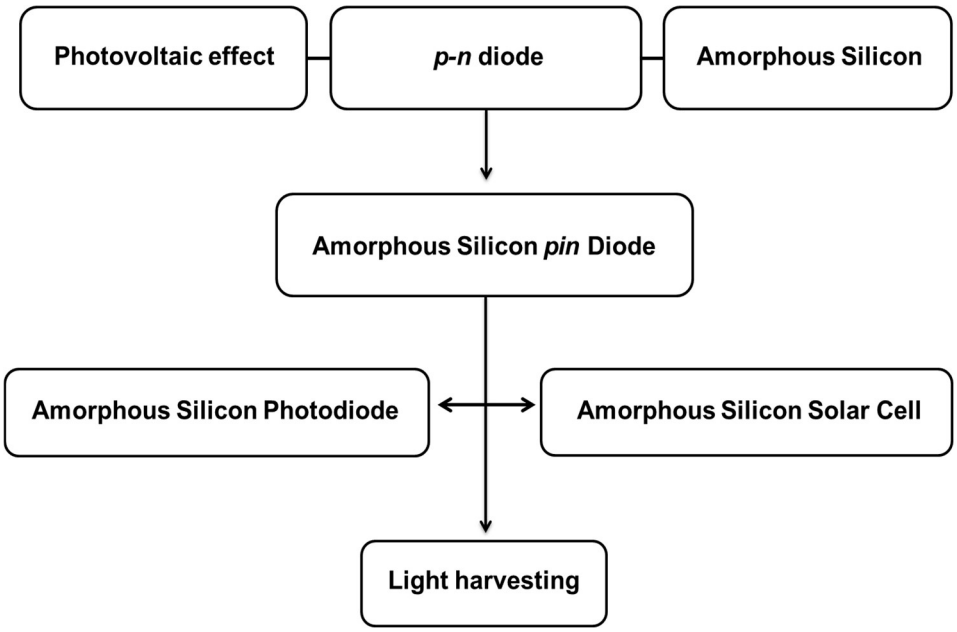

Figure 1. Overview of amorphous silicon thin film pin diode.

1.2 The photovoltaic effect

The fundamental physics of the operation of the pin diodes in this dissertation, which are used as solar cells or photodiodes, is based on the photovoltaic effect. Alexandre-Edmond Becquerel first discovered the photovoltaic effect in 1839 while investigating the effect of incident light on electrolytic cells.[4] The photovoltaic effect is true in semiconductor materials which have two discrete energy levels, i.e., valence and conduction bands, with a much smaller band gap than insulators. At 0 K, the valence band is filled by electrons and the conduction band is empty due to the absence of thermal energy.[5] At room temperature, some electrons occupy the conduction band due to the thermal energy. In this situation, if the light is illuminated on the semiconductor

materials and its energy is larger than the material band gap, electrons in the valence band are excited to the conduction band, which is commonly known as “the photovoltaic effect”. This mechanism is illustrated in Figure 2.

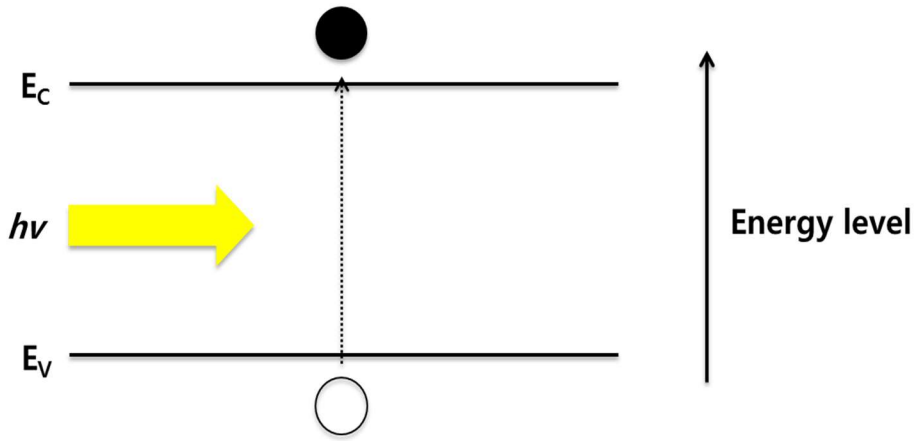

Figure 2. Band diagram of the photovoltaic effect (filled circle: electron and empty circle: hole)

1.3 Hydrogenated amorphous silicon

Silicon (Si) is the second most abundant semiconductor material on earth. Therefore, the a-Si:H can be an outstanding candidate for commercial applications such as solar cells or photodiodes.[6, 7] There are two typical configurations of Si atoms: crystalline silicon (c-Si) and amorphous silicon (a-Si). As shown in Fig. 3(a), the former is the well-ordered form of the Si atoms and the latter, shown in Fig. 3(b) is the non-crystalline form. This difference affects inherent material properties such as bandgap, conductivity, absorption coefficient, and so forth. It is well-known that the electrical

property of the c-Si is much better than that of the a-Si due to the well-arranged Si atoms.[8] Also, the c-Si absorbs a broad wavelength range of light, which is possible due to band gap that is smaller than that of the a-Si, e.g., 1.1 vs. 1.7 eV.[8] In spite of these advantages, the fabrication cost of the c-Si is hopeless because of the complicated manufacturing steps like the high level purification or singe crystalline growth.[8, 9] In contrast, the a-Si is inexpensive in the fabrication cost due to the availability of plasma induced deposition.

The a-Si contains many unbound states, known as "dangling bonds" that are approximately 10^{19} cm^3 in density,[10] which results in the poor property of the a-Si. The dangling bonds can be reduced by introducing hydrogen (H) atoms into the a-Si network, e.g., from 10^{19} to 10^{16} cm^3 in density, because the H atoms tend to passivate the dangling bonds, as shown in Fig. 3(c).[10] Once the dangling bonds are passivated by the H atoms, they do not act as defects anymore. Therefore, the H passivated a-Si is much more stable than the un-passivated a-Si.

The easiest way to form the a-Si:H is to use a plasma enhanced chemical vapor deposition (PECVD) technique. Therefore, most of the a-Si:H based devices, e.g., solar cell, thin film transistor, photodiode, and so on, have been deposited using the PECVD technique.[2, 11, 12] Normally, the deposited a-Si:H contain the H atoms of 5 - 10 atomic % and their quality is the best at the H content of about 10 atomic %.[8 13] At above 10% atomic % or more, the a-Si:H has the polymeric-like property due to the Si atoms bonding with two H atoms,[13] which causes micro-voids in the a-Si network and therefore the high defect density. To passivate the dangling bonds, it could be sufficient to use the

H atoms of only 1 atomic % or less.[8] In reality, however, this is impossible owing to the metastability of the a-Si:H. For example, without any external forces, (e.g. light or voltage bias), weak Si-Si bonds, dangling bonds, and H passivated bonds in the a-Si:H network are in a metastable equilibrium state.[13] In the presence of the external forces, however, the equilibrium is easily broken and the alternation between the equilibrium state and the non-equilibrium state is repeated, a process known as "metastability". This effect is easily observed when the a-Si:H is exposed to a light illuminated condition for a long period of time, referred to as "the Staebler and Wronski effect (SWE)".[14]

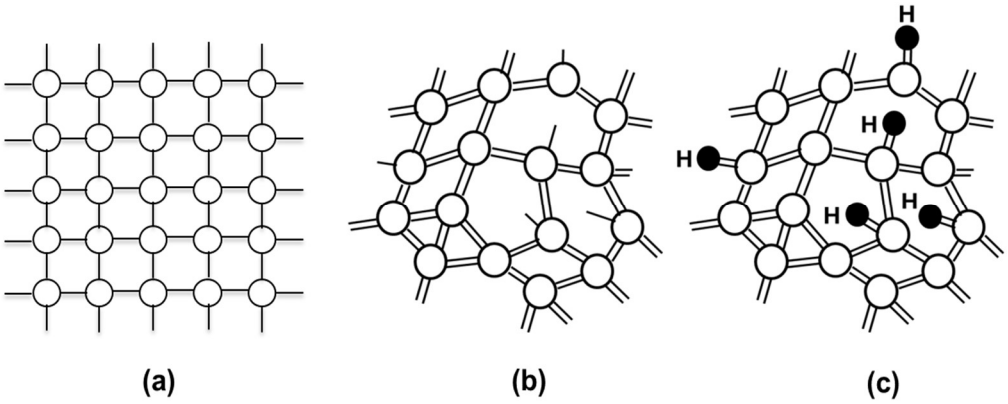

Figure 3. Atomic configurations of (a) crystalline silicon, (b) amorphous silicon, and (c) hydrogenated amorphous silicon.

1.3.1 Atomic configuration

A Si atom holds two electrons in 3s orbital and another two electrons in 3p orbitals. When Si atoms are close to each other, the electrons in the outermost orbitals,

i.e., 3s and 3p orbital, interact with those of the neighboring Si atoms. Then, the valence states of the Si atoms are separated into bonding and anti-bonding states. The former is lower than the valence states of the single Si atom because, in nature, the bonding formation lowers a material's total energy. This phenomenon indicates that the maximum number of the bonding states is a prerequisite in the formation of the Si network. Si is optimum in the four-bonding formation. Therefore, its outermost orbitals, i.e., 3s and 3p orbitals, are hybridized into four sp^3 hybridized energy states, forming four Si-Si bonds.

Figure 4 shows atomic bonding models of (a) c-Si, (b) a-Si, and (c) a-Si:H. The c-Si of Fig. 4(a) possesses the constant atomic angle (109° 28') and length (0.235 nm) between the neighboring Si-Si bonds thanks to the well-organized atomic structure.[8] In the un-passivated a-Si in Fig. 4(b), the bonding angles are distributed with the standard deviation of 6-9° and the bonding lengths are randomly varied by approximately 0.235 nm.[8, 15] The H passivation is not responsible for changing the bonding angle and length in the a-Si:H network, as shown in Fig. 4(c).

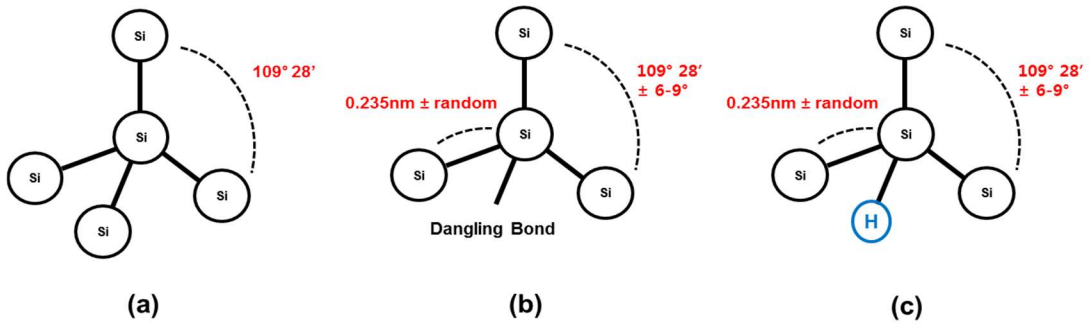

Figure 4. Atomic bonding models of (a) crystalline silicon, (b) amorphous silicon, and (c) hydrogenated amorphous silicon.

1.3.2 Substitutional doping

The substitutional doping of boron (B) for p-type property or phosphorous (P) for n-type property in a-Si:H network can be done by the mixing diborane (B_2H_6) or phosphine (PH_3) with silane (SiH_4) during a PECVD process. This work was first demonstrated by Spear and Le Comber in 1975.[16] Physically, the addition of the dopants to the a-Si:H network shifts the Fermi level toward the E_C or E_V, depending on the dopant character.[17] This directly changes the conductivity of the a-Si:H together with the activation energy. The activation energy of the undoped a-Si:H is 0.7-0.8 eV and that of the P- or B-doped a-Si:H is 0.15 or 0.3 eV, separately.[18]

The doping efficiency in the a-Si:H is as follows:[8]

$$\frac{[D_{active}]}{[D_{total}]} \approx C \frac{1}{\sqrt{[D_{total}]}} \quad [1]$$

where [D_{active}] is the concentration of the ionized dopants, [D_{total}] is the total concentration of dopants, and C is the constant. In the a-Si:H, the doping efficiency is inversely proportional to the total concentration of the dopants. In other words, its increase is not guaranteed with the increase of the dopant concentration. As stated previously, the Fermi level shifts toward the band edge, i.e., E_C or E_V, according to the doping concentration and property of the dopant. In the a-Si:H, however, this phenomenon is disturbed due to the band tails near the E_C and E_V.[18] In this situation, the maximum doping efficiency is determined by the dopant property. For instance, the doping efficiency of the B atoms is lower than that of the P atoms because the width of valence band tail is wider than that of the conduction band tail.[8] Separately, the doping process generates additional dangling bonds, which is another indication that the increase of the dopant concentration causes a decrease in the doping efficiency.

All atoms in the a-Si:H network are formed in the optimal bonding configuration, according to the 8-N rule. This rule states that the atomic bonding formation is as follow: the maximum number of electrons participate in the bonding formation, the remaining electrons leave unbound states, and anti-bonding states are empty.[18, 19] Based on this principle, the doping of the P and B atoms proceeds in the a-Si:H network. For instance, a P atom has two electrons in the 2s orbital and three electrons in 2p orbitals. The three electrons in the outermost 2p orbital have three-fold coordination to bond with the Si atoms. Once they make the bonding formation, the two electrons in the 2s orbital occupy the highest valence band. The number of the optimum bonds of the P atom is four. Therefore, one electron in the 2s orbitals generates the additional bonding formation

with the neighboring Si atom while breaking the weak Si-Si bonds. Consequently, the inactive P atom is ionized, becoming a negative ion. The remaining one electron is promoted to the anti-bonding state and becomes a free carrier. The doping process of the B atoms in the a-Si:H is similar with that of the P atoms.

1.3.3 Electronic states in a-Si:H

Figure 5 shows the density of state (DOS) of the a-Si:H. The a-Si:H has different electronic environment from the c-Si. In addition to extended states, there are the band tails which are composed of localized states in the band gap, as shown in Fig. 5. The band tails are located near the edge of the valence and conduction bands and their width is known to be Urbach energy.[20] Due to this feature of the a-Si:H, the band gap between the E_V and the E_C is called the "mobility gap", which differs from the forbidden band gap in the c-Si. The former is typically 1.7-1.8 eV, whereas the latter is 1.1 eV. The density of the band tail states decrease exponentially toward the middle of the band gap. For the valence band tails, the DOS is proportional to $\exp\{\frac{E_V-E}{E_V^0}\}$. For the conduction band tails, it is proportional to $\exp\{\frac{E_C-E}{E_C^0}\}$, where E_V^0 and E_C^0 are energy constants for exponential functions. The E_V^0 and E_C^0 are dependent on the degree of the structural disorder in the a-Si:H. Note that the localized states in the band tails act as traps, different from recombination centers. Therefore, they capture and thermally release free carriers. This mechanism is repeated in the presence of the external forces, e.g., light or electrical bias condition.

The dangling bonds in the a-Si:H are attributed to the midgap states. Therefore, the number of the midgap states is affected by the H passivation. The more the H passivation of the dangling bonds is, the less the midgap states are. Once the dangling bonds are passivated, they are not the recombination centers anymore. According to the Pauli exclusive principle, each energy state can be occupied by up to two electrons. Each dangling bond holds one electron. Therefore, the dangling bond state is said to be a neutral state (expressed as D^0). The dangling bond state holding two electrons corresponds to D^-. If there is no electron in the dangling bonding state, it is D^+. The charge transition between the neutral dangling bonds is shown by the follow equation:[18]

$$2D^0 \leftrightarrow D^+ + D^-$$

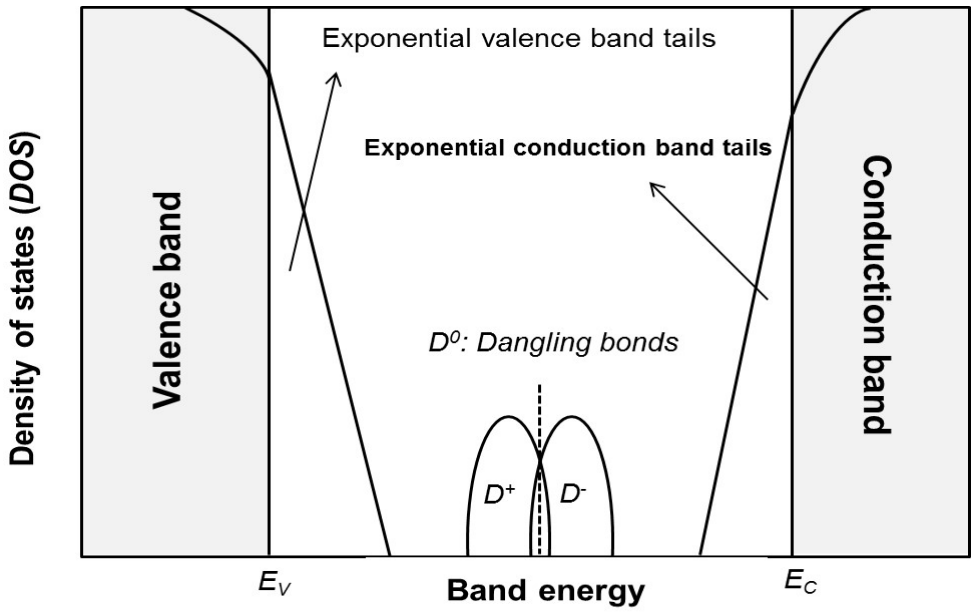

Figure 5. Electronic density of state in a-Si:H.

1.3.4 Carrier transport mechanism

Present in the a-Si:H are three carrier transporting paths: (1) the extended states, (2) band tail states, and (3) Fermi energy states.[18] In the extended states, the carrier transport is contributed by the thermal activation of carriers from E_F to E_C, as the following relation:

$$\sigma_{ext} = \sigma_{oe} \exp\left[-\frac{E_C - E_F}{kT}\right] \quad [2]$$

Where σ_{oe} is the average conductivity in the extended states, $\sigma_{ext}$is the extended state conductivity, k is the Boltzmann constant, and T is the absolute temperature. $E_C - E_F$ is the activation energy dependent on the Fermi energy level.

In the band tail states, the carrier transport is carried out by the hopping process via the localized states, which is expressed by the following equation:

$$\sigma_{bandtail} = \sigma_{ot} \exp\left[-\frac{E_{CT} - E_F}{kT}\right] \quad [3]$$

Where σ_{ot} is the average conductivity in the localized states, $\sigma_{bandtail}$is the conductivity in the band tail states, and E_{CT} is the average energy of the localized states.

In the Fermi energy states, the carrier tunneling process is dominant in the dangling bond states. This mechanism is only possible when the number of the dangling bond states is large enough. If the density of the dangling bonds decreases due to the H passivation, the carrier transport at the Fermi level states will be suppressed.

1.3.5 Band structure of a-Si:H

It is well-known that the GaAs has a direct band gap and the c-Si has an indirect band gap, which are well defined by the energy (E) and momentum (k) dispersion relationship.[18] In the a-Si:H, there is no distinction between the former and the latter because the k cannot be conserved. In comparison to the c-Si in which the electron wavefunction is well-extended, i.e., a long traveling range, the a-Si:H localizes the electron wavefunction due to the electron scattering caused by the disordered atomic structure. Therefore, the E and k relationship cannot be applicable to the a-Si:H. The optical transition of the a-Si:H occurs from the overlap between the energy states in real space.

1.3.6 Light-induced degradation

The a-Si:H is deteriorated by a prolonged exposure to light illumination or electric bias,[14, 21] the aforementioned "Staebler-Wronski effect (SWE).[14] Physically, non-radiative energy, which is released from the carrier recombination, is transferred to H atoms. The H atoms then break weak Si-H or Si-Si bonds and generate the dangling bonds.[22] This kind of the defect generation follows the stretched exponential behavior over time.[23] The light- or electric-stress induced defects can be restored to their original state after the heat treatment of 10-100 min at 130-200°C.[14, 21, 24] This process is related to the length of the H diffusion.[8] If the annealing temperature is higher than the critical temperature in which the H diffusion length reaches around 1 Å, the defect recovery process can be predominant.

1.4 p-n diode

The foremost requirement for the applications of the a-Si:H pin diode, such as a-Si:H solar cells and photodiodes, is a current rectifying behavior. As shown in Fig. 6, the electrical current rarely flows in negative bias ranges, whereas it flows rapidly in positive bias ranges. This situation is possible due to the formation of the p-n junction, first observed in 1939 by Russell Shoemaker Ohl.[25]

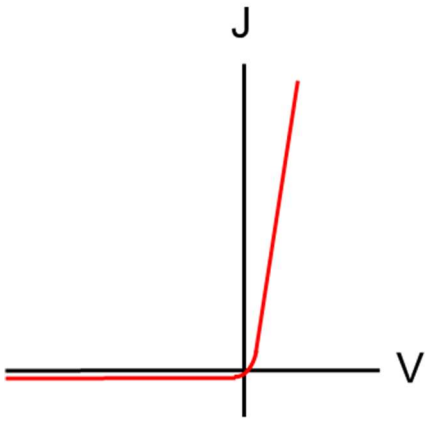

Figure 6. I-V characteristic of p-n junction.

As shown in Figure 7, when a hole-rich p-type semiconductor combines with an electron-rich n-type semiconductor, two kinds of carrier flows are generated in the opposite direction; (1) diffusion and (2) drift current. The former is from the carrier concentration gradient and the latter is from the internal electric field. In detail, alongside the junction between the p- and n-type semiconductors, holes diffuse from the

p-type to the n-type semiconductor while leaving acceptor ions in the p-type semiconductor, and electrons diffuse from the latter to the former while leaving donor ions in the n-type semiconductor. This carrier exchange process originates from the carrier concentration gradient between the p-type and n-type semiconductors. At the same time, the ionized region generates the internal electric field (V_0), which causes the transport of minor carriers in the opposite direction as the carrier diffusion. This process is kept until the Fermi level between the p and n type semiconductors is pinned, i.e., the net current is zero (in other words, diffusion current = drift current). After all, the space charge region known as the "depletion region" in which few carriers exist is formed in the middle of the p-n junction. The V_0 within the depletion region is determined by the following equation:[5]

$$\frac{p_p}{p_n} = \frac{n_n}{n_p} = e^{qV_0/kT} \quad [4]$$

where p_p and p_n are the hole and electron concentration in p-type semiconductor, separately, n_n and n_p is the electron and hole concentration in n-type semiconductor, separately, q is the charge, k is the Boltzmann constant, and T is the absolute temperature.

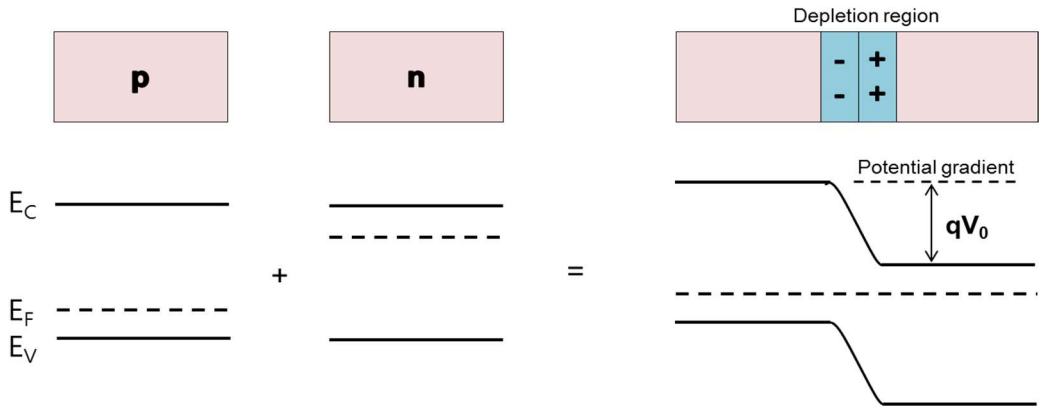

Figure 7. Formation of p-n junction in band diagram.

Figure 8(a) shows the p-n diode under no applied voltage. Without any external force, a semiconductor system tends to keep the thermal equilibrium state, i.e., the relationship of $pn = n_i^2$, where n_i is the intrinsic carrier concentration.[26] Under the positive bias, the depletion region of the diode is reduced, as seen in Fig. 8(b), which lowers the barrier height with the decrease of the internal electric field, i.e., V_0 - V_F. Therefore, the injection current easily flows through the p-n diode. Furthermore, pn is larger than n_i^2 throughout the p-n diode because of the carrier injection from an external source. To reach the condition of $pn = n_i^2$, the recombination current is dominant in the positive bias. On the other hands, under the negative bias, the depletion region is expanded and the pn is smaller than n_i^2 across the diode due to the carrier collection of the external source, as shown in Fig. 8(c). Therefore, few carriers in the extended depletion region are thermally generated and participate in the current flowing through the diode.

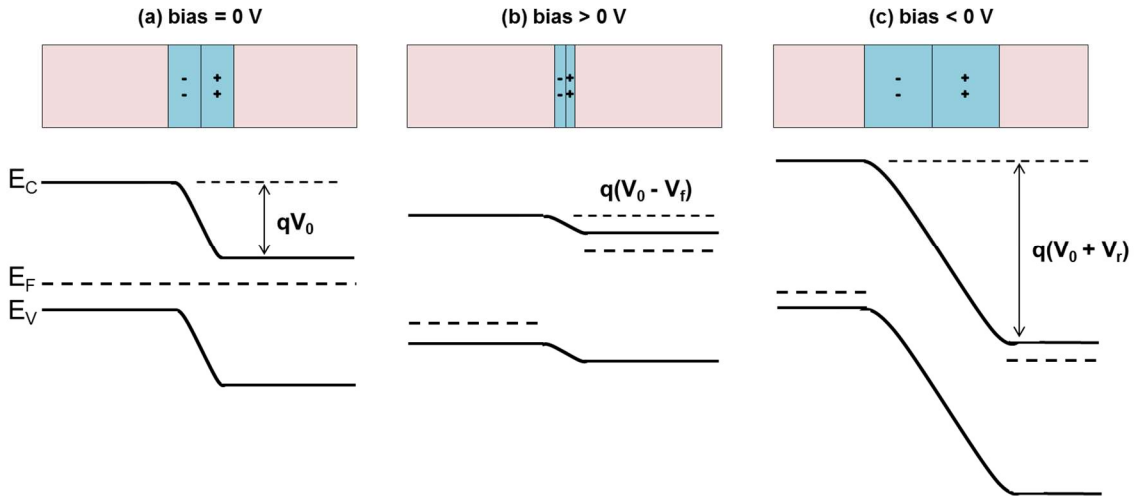

Figure 8. Band diagram of p-n junction under (a) bias = 0V, (b) bias > 0V, and bias < 0V.

1.5 pin diode

Since the traditional p-n diode is not effective in harvesting lights, the pin structured diodes in Fig. 9(a) have been mostly employed for the a-Si:H solar cells or photodiodes.[12, 27-29] The intrinsic (i)-a-Si:H layer embedded between the p and n type a-Si:H layers enhances the absorption of the incident light and therefore the photocurrent. Normally, the i-a-Si:H is much thicker than the doped layer, i.e., 150-300 vs. 10-20 nm, so that its light absorption efficiency is as high as possible. As shown in Fig. 9(a), the diode keeps the thermal equilibrium condition when it is in the open-loop circuit condition. If the diode is in the closed-loop circuit condition, as drawn in Fig. 9(b), the potential gradient across the i-layer appears. In this situation, if the incident light is absorbed through the diode, photo carriers are generated and then guided by the internal electric field. Note that the carriers generated in the doped layers, i.e., p- or n-type layer,

immediately recombines with the opposite signed carriers because of the absence of the internal electric field.

To improve the electrical performance of the pin diode, a window layer, i.e., a doped layer closest to a light source, should be well-designed. The window layer should be as thin as possible while keeping the internal electric field properly across the diode. Otherwise, the loss of the incident light will be serious. This will decrease the light absorption efficiency of the i-layer, eventually lowering the diode performance. Also, the light loss in the window layer is affected by the doping concentration in the i-layer; the increase of the doping concentration corresponds to the increase of the defect states. Another way to reduce the loss of the light is to use a high band gap material like amorphous hydrogenated silicon carbide (a-SiC:H).[30]

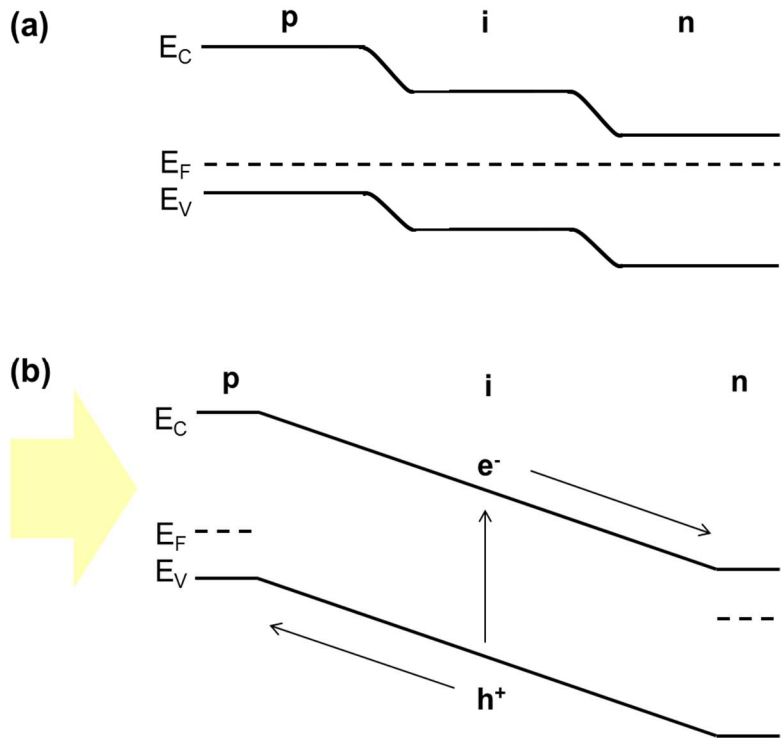

Figure 9. Band diagram of (a) pin diode under open-loop condition and (b) light-illuminated pin diode and its carrier collection mechanism under closed-loop condition.

1.6 Outline of this dissertation

Chapter II details the overall information on device fabrication and characterization. It also introduces the pin tri-layer deposition technique and the fabrication process of the pin diode used for the solar cell and photodiode applications. The chapter describes the experimental method used to investigate the optical property of the pin diode will be shown. Finally, it provides a discussion of the diode characterization.

Chapter III focuses on the effect of film deposition sequence on the performance and stability of a-Si:H solar cells. The chapter also compares the stress techniques for studying the solar cell reliability.

Chapter IV explains how the light detection of the pin diode depends on the light wavelength and power density. Also discussed is the light absorption efficiency of the a-Si:H tri-layer. Also, important factors affecting diode properties, such as open-circuit voltage (V_{OC}), short-circuit current density (J_{SC}), internal resistance, or back reflector will be investigated with respect to the light wavelength and power density.

Chapter V discusses the effect of the i-layer thickness on the light-detection property of the a-Si:H pin diode. The chapter shows that defect density in the i-layer affects the wavelength dependence of the light-sensing of the diode. The chapter also explains a related mechanism using the combined electric-light illumination stress technique.

CHAPTER II

EXPERIMENTAL

2.1 Plasma enhanced chemical vapor deposition

2.1.1 Plasma

Plasma is defined as the form of partially ionized gas composed of the same numbers of positively charged ions and negatively charged electrons, called quasi-neutrality, and two different species in ground or excited state.[31] It always exists in a non-equilibrium state in which the electrons and ions are more dynamic than neutral species. This is different from normal gas states, such as liquid, solid, and gas. Therefore, the plasma is expressed as a "fourth state of matter".

2.1.2 Collision processes: elastic and inelastic collisions

In the PECVD process, the plasma is triggered by the coupling of the electric field and the free electrons in feeding gases. High energy electrons collide with neutral species, leading to the ionization of the neutral species. The collision processes come in two types, (1) elastic and (2) inelastic collisions of energetic electrons.[32] In the former, while colliding with neutral or ionized particles, the electrons conserve their energy and momentum and thus, no energy transfer takes place. In the latter, during the collision, the energy and momentum of accelerated electrons are transferred to atoms or ions. In this situation, two important processes take place in the plasma, (1) ionization and (2) excitation. Ionization is caused by the collision of energetic electrons to atoms. For

example, when one electron hits one argon (Ar) atom, two electrons are formed along with positively ionized Ar:

$$e^- + Ar \rightarrow Ar^+ + 2e^-.$$

Excitation is caused when an atom or an ion is excited by the electron collision:

$$e^- + Ar \rightarrow Ar^* + e^-.$$

The excitation lifetime is very short. During the relaxation of the excited states, photons are emitted. Such emission is referred to as “glow discharge”, i.e., “plasma”.

2.1.3 Plasma-induced deposition process

The plasma, which is generated during the PECVD deposition process, contains two different phases, (1) charged ions and electrons and (2) neutral radicals, atoms, and molecules.[33] The former is driven by ion acceleration when transporting to a substrate surface, whereas the latter is driven by diffusion. The surface reaction then occurs with the adsorption of reactants to the substrate surface, which is affected by complicated functions of ion bombardment, reactant, temperature, and so forth. The by-products remaining after the reaction are desorbed from the substrate surface and are discharged out of the PECVD reactor.

For the formation of a-Si:H film in the PECVD system, SiH_4 gases are typically utilized as a parent gas. The plasma generation in the SiH_4 environment causes the decomposition of the SiH_4 molecules with the collision of field-accelerated electrons and then produces neutral radicals such as SiH_3, SiH_2, SiH, Si, H and emissive species SiH^*, Si^* and other ions [34] Among those species, the SiH and SiH_2 radicals are highly reactive, compared to the SiH_3 radicals.[35] They move to a given substrate, diffuse through the a-Si:H film, react with H atoms on the surface, and then leave the surface. Therefore, the SiH_3 radicals are a main precursor for the deposition of high quality a-Si:H films.[36] They react with surface dangling bonds and form Si–Si bonds.

2.1.4 pin structure fabrication

A Corning 1737 glass was chosen as a substrate. Before film formation, it was cleaned according to the following procedure: (1) 10 min of ultra-sonication of the glass in de-ionized (DI) water with 18 MΩ-cm, (2) rinsing using acetone to remove the contaminants, (3) additional rinsing using isopropanol alcohol to remove the acetone residue, and (4) rinsing using DI water and then drying the glass. For the formation of a bottom electrode, an 80 nm thick ITO film or 200 nm thick Mo film, which depends on an experiment design, was sputter-deposited using an ITO target (In2O3: SnO2 = 9:1) in a sputtering system with a 13.56 MHz RF generator (ENI, OEM-650) with an automatic matching network at 80 W, 5 mTorr in Ar for 40 min. All pin tri-layers in this dissertation were deposited in a single chamber type PECVD (Applied Material, AMP Plasma I) with the configuration of a parallel electrode with 64.5 cm in diameter and

6.25 cm in the gap between the electrodes. The top electrode of the PECVD chamber was powered and the bottom electrode and chamber wall were grounded. The film deposition power was managed from a 13.56 MHz (OEM-12A, ENI) RF generator with a pi-type matching network (MW-10, ENI) or 50 kHz RF generator with an automatic matching network. The control of deposition parameters, such as deposition pressure, power, and parent gas flow rate (using mass flow control systems) was performed by a PC with LabWindow/CVI interface (National Instrument). Figure 10 shows the simplified diagram of the PECVD reactor. In order to deposit an a-Si:H film, firstly, a 1737 Corning glass was loaded into the reactor and the reactor was evacuated to reach a high vacuum environment using a mechanical pump. When the background pressure in the reactor was set, process gases were supplied to the reactor; SiH4 (semiconductor, 99.999% Air Liquide), B_2H_6 (2 % in H_2, 99.999% purity, Air Liquide), PH_3 (7.1 % in H_2, 99.999%, Air Liquide), and H_2 (semiconductor, 99.9999% purity, Praxair). After reaching a desired deposition pressure, RF power is applied to the top electrode, which generated the plasma. Eventually, the desired a-Si:H film is formed on the 1737 glass substrate.

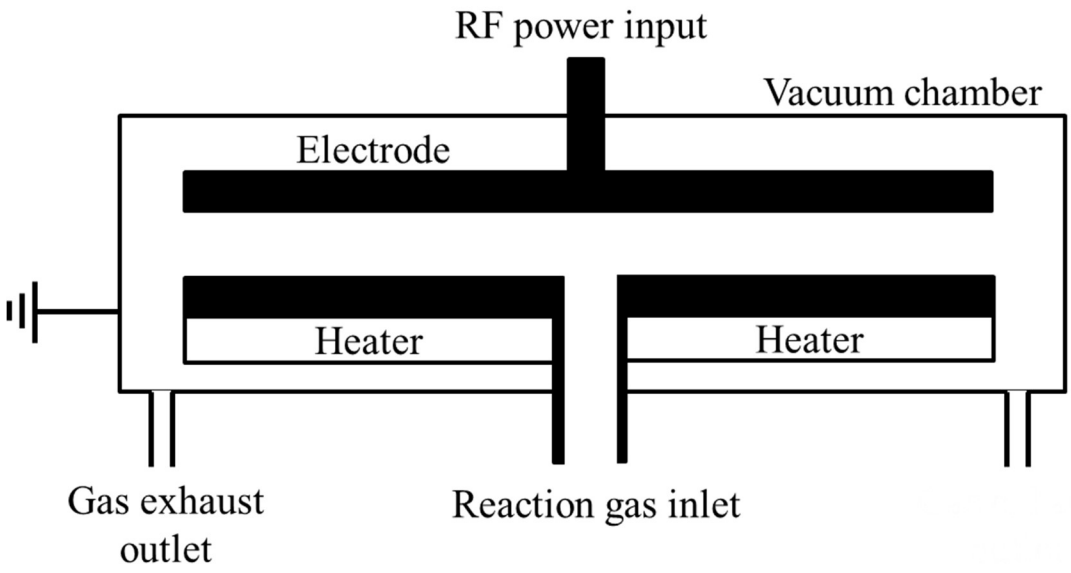

Figure 10. Simplified PECVD reactor.

2.1.5 Patterning process (lithography)

To complete the fabrication of solar cells and photodiodes used in this dissertation, the patterning step of the top ITO electrode was required. For the patterning process, at first, a negative photoresist (NPR) (AZ Electronics, AZ 2020) was spin-coated on the top of pin a-Si:H tri-layer using a spin coater (Chemat Technology, KW-4A; Fig 11(a)), followed by 90 ℃ soft-bake to dry solvent residue and enhance the NPR adhesion. The spin speed was set to 4000 RPM to disperse the NPR, creating a layer of approximately 1.4-1.5 μm in thickness. The soft-baked sample was exposed to the UV light (7 mW/cm^2) using the mask aligner (Quintel, Q4000) equipment in contact mode for 30 s (Fig 11(b)), followed by the second soft-bake at 90 ℃. The non-exposed NPR area was developed in a solution made of developer (AZ Electronics, MIF 300) and DI

water in a 3:1 ratio (Fig 11(c)). To firm the NPR, the NPR patterned sample was hard-baked in a 125 °C oven for 5 min. The ITO film not protected by the NPR was etched in aqua regia solution made of HNO_3 : HCl (1:3) (Fig 11(d)). Finally, the NPR residue was removed by the acetone in an ultrasonic bath for 1 min (Fig 11(e)).

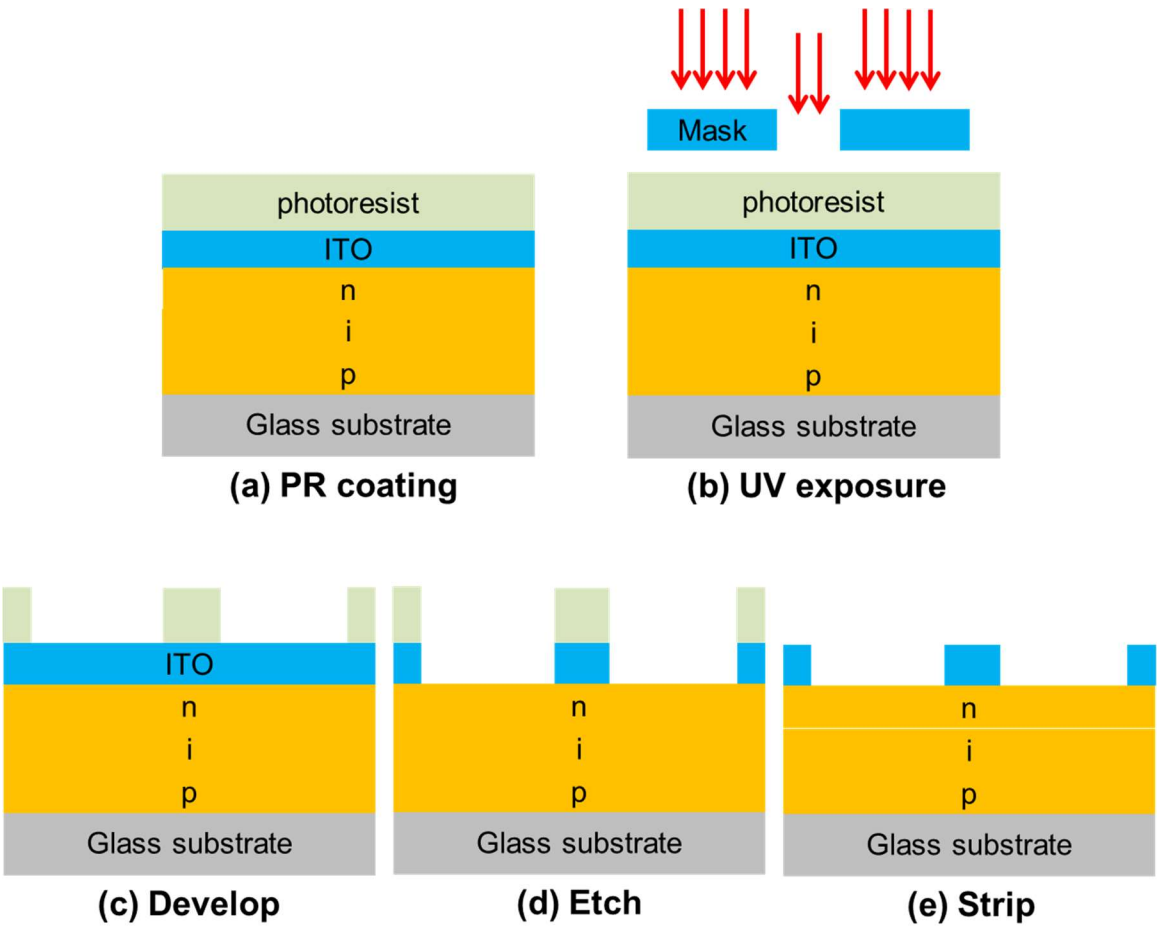

Figure 11. ITO Pattering process.

2.2 Optical and electrical property characterization

2.2.1 Optical characterization

To investigate the light absorption efficiency of a-Si:H films with different wavelength illumination lights, the studies in the dissertation used mono-wavelength lights as light sources, i.e., red (625 nm, M625L3, 1.98 eV), green (530 nm, M530L3, 2.34 eV), and blue (470 nm, M470L3, 2.64 eV) from Thorlabs. These lights have greater photon energy than the a-Si:H, i.e., 1.7 eV. Figure 12 shows the experimental setup to measure the transmitted light through the a-Si:H film. The light transmitted through the a-Si:H film is collected by a digital power meter (PM100A, Thorlabs) positioned underneath the film. Regarding experimental goals, the power density of the light varies with 0.705, 1.411, 2.822, 4.232, or 5.643 mW/cm^2.

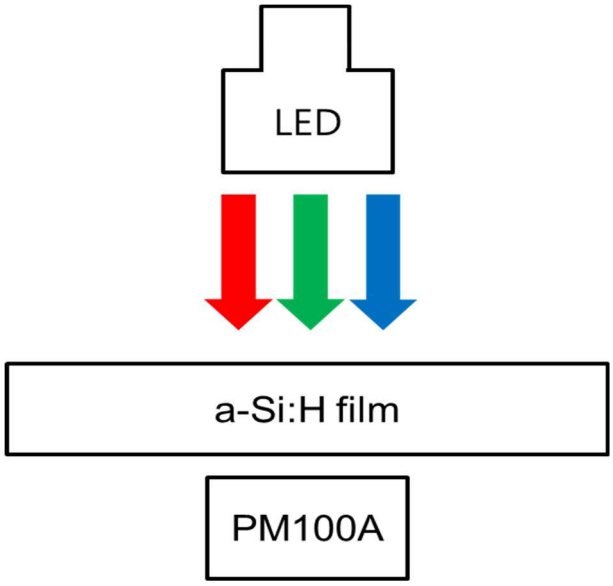

Figure 12. Optical measurement setup

2.2.2 Electrical property characterization

Current density (J) – voltage (V) characteristics of the pin solar cell and photodiodes are measured by the Agilent 4140B parameter analyzer under AM 1.5G solar light illumination from a solar simulator (Solar Light Co., Model: 16S-300-002) at room temperature in a black probe station. The measurement of the pin devices is carried out from a voltage sweep from -2V to 2V under the light illuminated condition. Then, from the J-V characteristic, the parameter extraction is calculated. This calculation indicates, as shown in Fig. 13, the device performance, such as short-circuit current density (J_{SC}), open-circuit voltage (V_{OC}), fill factor (FF), power conversion efficiency (PCE), external quantum efficiency (EQE), series resistance (R_S), and shunt resistance (R_{sh}).

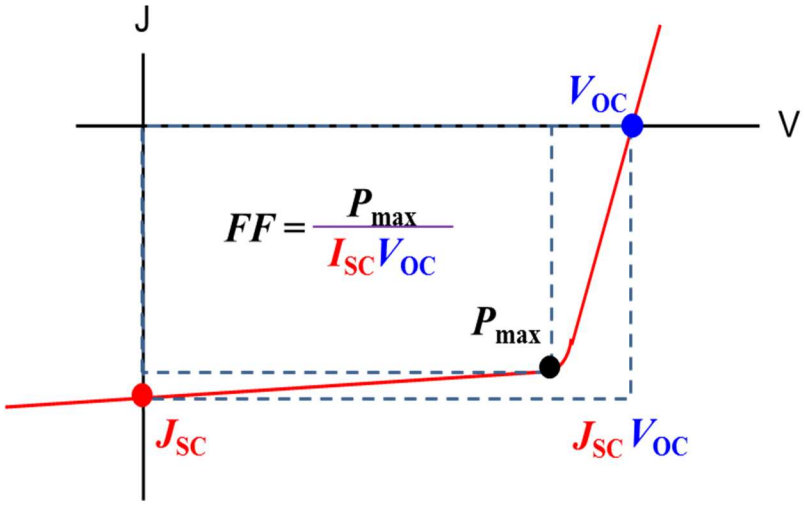

Figure 13. Current density (J) – voltage (V) characteristic of the a-Si:H pin diode under light illumination.

2.2.1 Short-circuit current density

The J_{SC} is defined as photocurrent (J_{ph}) flowing through the diode at no external voltage, i.e., when V = 0, as shown in Fig. 13. In ideal diodes, the J_{SC} has to be equal to the J_{ph} because the loss of internal photocurrent is negligible. However, it is difficult to avoid the internal current loss in real diodes. The theoretical maximum of the J_{SC} is dependent on the number of photo-generated electron-hole pairs per unit time and material band gap.[8] The J_{SC} increases with the decrease of the band gap. This is an indication that the property of the a-Si:H pin diode cannot exceed that of the c-Si diode.

2.2.2 Open-circuit voltage

In Fig. 13, the V_{OC} can be obtained when current flow across the diode is zero. It estimates the magnitude of the internal electric field across the i-layer. Normally, the V_{OC} is predicted by the following relation[8]:

$$V_{OC} = \frac{nkT}{q} \ln\left(\frac{J_{ph}}{J_0}\right) \quad [5]$$

where J_0 is the dark saturation current, q is the electron charge, n is the diode quality factor, k is the Boltzmann's constant, and T is the absolute temperature. According to Eq. 5, the V_{OC} is dependent on the diode quality, temperature, as well as, photocurrent density.

2.2.3 Fill factor

The FF is defined as the ratio of the experimental maximum power (P_{max}) of the light-illuminated diode to ideal maximum power (I_{SC} x V_{OC}), as shown in Fig. 13. Graphically, the P_{max} corresponds to a small quadrangular area, whereas the ideal maximum power corresponds to a large quadrangular area. The smaller the area difference is, that is, a high FF, the better the diode performance is.

2.2.4 Power conversion efficiency

The real light-to-electricity conversion efficiency of the diode is expressed by the PCE, which is calculated through Eq. 6. Its definition is the ratio of the experimental maximum power density to the incident light power density.[37] The PCE is determined by multiple contributions of the J_{SC}, V_{OC}, FF, and incident light power density.

$$PCE = \frac{P_{d,max}}{E_e} = \frac{FFJ_{SC}V_{OC}}{E_e} \quad [6]$$

where $P_{d,max}$ is the experimental maximum power density of the diode and E_e is the incident light power density.

2.2.5 External quantum efficiency

The EQE, defined as the ratio of collected electron-hole pairs to an incident photon, differs from the PCE. It is the most useful parameter when studying the diode

performance on lights of mono-wavelength, which can be easily calculated from the following equation[8]:

$$\mathrm{EQE} = \frac{|\frac{J_{SC}}{q}|}{E_e/\frac{hc}{\lambda}} \qquad [7]$$

2.2.6 Internal resistance

The internal resistances in a-Si:H pin diodes are of two types, R_s and R_{sh}. The former is associated with material's bulk resistance and the latter is associated with current leakage within the diode.[38] These resistances can be estimated from the J-V curve in Fig. 14. The R_S is proportional to the inverse slope of the curve at the V_{OC} and the R_{sh} is proportional to the inverse slope of the curve at the J_{SC}. In a high quality diode, the R_s should be small and the R_{sh} should be large, since the bulk resistance and current leakage influenced by trapping or recombination centers, e.g., localized state or dangling bond, is small.

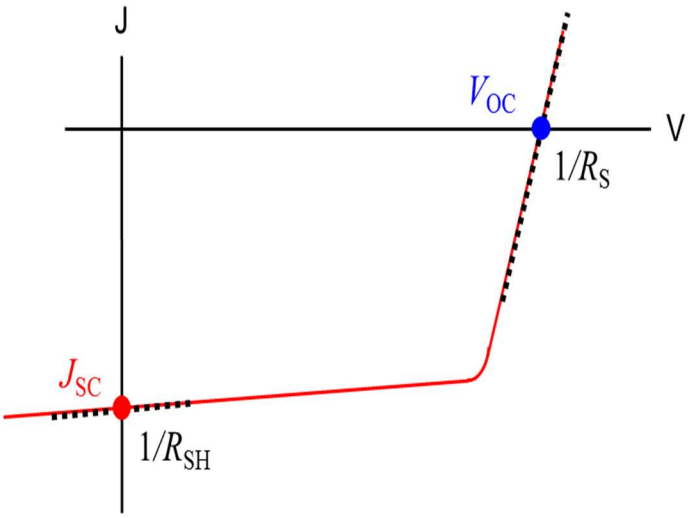

Figure 14. Shunt (R_{sh}) and series resistance (R_S) of the a-Si:H pin diode under light illumination.

CHAPTER III

INFLUENCE OF PIN AMORPHOUS SILICON STACK DEPOSITION SEQUENCE ON SOLAR CELL PERFORMANCE AND DEGRADATION[1]

3.1 Introduction and motivation

The Staebler-Wronski effect (SWE), which stated the creation of metastable defects in the hydrogenated amorphous silicon (a-Si:H) under the prolonged light exposure, was first reported in 1977.[14] These defects are generated from the breakage of weak Si-H or Si-Si bonds accompanied with the migration of hydrogen (H) atoms.[22] Separately, it was reported that when the same number of boron (B) and phosphorus (P) dopants were included in the same a-Si:H film, the defect density in the film was reduced and the SWE was attenuated.[39] However, when the a-Si:H film was doped with only B or P, the SWE phenomenon was more serious than that in the intrinsic a-Si:H film.[40, 41] This effect was further enhanced with the increase of the dopant concentration.[40, 41]

The SWE in a-Si:H is dependent on the light illumination time.[24, 42, 43] Separately, when an a-Si:H nip cell is stressed with a forward current, its performance deteriorates.[21] It appears that the defect creation mechanism under the current-stress condition is similar to that under the light illumination condition. The a-Si:H cell deteriorated from

---

[1] Data reported in this chapter is reproduced from "Influence of pin Amorphous Silicon Stack Deposition Sequence on Solar Cell Performance and Degradation", by Kibum Kim and Yue Kuo, published by ECS Journal of Solid State Science and Technology, 6(1), Q29-Q33 (2017), and by permission of ECS.

the electric-stress could be restored to its original state after being annealed at a temperature higher than 150°C.[14, 21]

A-Si:H solar cells with the pin or nip tri-layer structure prepared by the PECVD process in the same chamber usually suffers from the unintentional contamination of the i-layer from the dopant residue left from the prior film deposition step.[8, 44-47] The dopant contamination of the i-layer has also been observed in the multi-chamber PECVD process where the dopant diffusion occurred from the plasma-induced damage to a previous deposited thin film during the i-layer deposition.[8] Since the material properties of the i-layer is critical to the cell performance, the deposition sequence of the a-Si:H tri-layer can affect the cell's electrical and optoeletrical characteristics.[48] Consequently, the stability of the cell under the light- or electric-stress condition is affected by the deposition sequence of the tri-layer stack. In this chapter, the performance and deterioration of a-Si:H solar cells with the pin and nip stacked structures prepared in the same chamber will be investigated. The influence of the tri-layer stack on the damage recovery using the thermal annealing method will be also studied.

3.2 Experimental

A 200nm thick Mo layer was sputter-deposited on the Corning 1737 glass as the bottom electrode. The a-Si:H pin or nip tri-layer was deposited at 260°C within the same PECVD chamber with a 13.56MHz RF power supply in one pump-down without breaking the vacuum. Deposition conditions of all layers are summarized in Table 1. Prior to the deposition of the i-layer, the chamber was purged twice with Ar and then

evacuated to a high vacuum to remove the dopant gas left from the previous deposition step. The PECVD (Applied Materials, AMP Plasma I) chamber has a parallel electrode configuration: the top electrode has a diameter of 64.5 cm and the bottom electrode has the same diameter as the top electrode except a 2.5 cm diameter exhaust hole in the center. An 80 nm thick ITO layer was sputter-deposited on the top of the pin or nip stack and subsequently wet-etched into 2 mm diameter top electrodes. The complete cell was annealed at 200°C for 30 min in air. For the reliability study, the electrode in contact with the p^+ layer was stressed at 5V in dark or under the illumination of AM 1.5G solar light (Solar Light Co., Model: 16S-300-002) at room temperature.

Table 1. Deposition condition of pin or nip a-Si:H films

	Gas ratio				Thickness	Power	Pressure	Temp.
	SiH_4	H_2	B_2H_6	PH_3	(nm)	(W)	(mTorr)	(℃)
p^+	35	400	20	0	15	50	700	260
i	60	0	0	0	300	100	400	260
n^+	60	1000	0	20	20	300	800	260

3.3 Influence of tri-layer deposition sequence on solar cell performance

Figure 15 shows structures of the a-Si:H solar cells with the (a) pin and (b) nip tri-layers. Due to the incomplete removal of the dopant residue left from the previous

thin film deposition, the i-layer in the pin stack is actually a p^- layer and the i-layer in the nip stack is an n^- layer.[44-47] The lightly doped i-layer causes the shift of the junction at the i-n^+ (in $p^+p^-n^+$) or i-p^+ (in $n^+n^-p^+$) interface, which affects the solar cell function. According to literature reports,[48-50] the $p^+p^-n^+$ cell has a higher solar cell efficiency than the $n^+n^-p^+$ cell mainly due to the higher V_{OC}. This is because the injection current in the $p^+p^-n^+$ cell is lower than that in the $n^+n^-p^+$ cell under the forward bias condition.[48] The Table 2 result shows that in addition to the higher V_{OC}, other solar cell characteristics of the $p^+p^-n^+$ cell are better those of the $n^+n^-p^+$ cell. Since corresponding individual layers of the tri-layer in both cells were deposited under the same condition, the unintentional doping of the i-layer can be an important factor for the performance difference.

Table 2. Initial efficiency of $p^+p^-n^+$ and $n^+n^-p^+$ cells

sample	J_{sc} (mA)	V_{oc} (V)	FF (%)	Eff. (%)
$p^+p^-n^+$ cell	7.97	0.87	50	3.4
$n^+n^-p^+$ cell	6.03	0.71	47	2.0

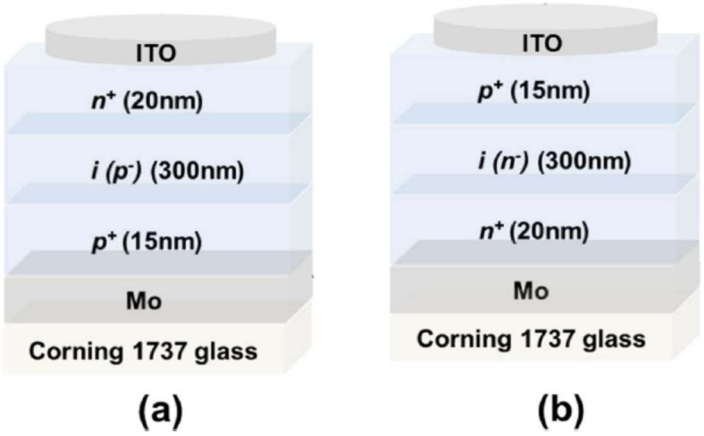

Figure 15. Schematic structures of (a) pin ($p^+p^-n^+$) and (b) nip ($n^+n^-p^+$) structured solar cells.

The electrode contact property can also be influenced by the film deposition sequence, which affects the cell's characteristics. For the cell with the $p^+p^-n^+$ stack, the p^+ layer is in contact with the bottom Mo electrode and the n^+ layer is in contact with the top ITO electrode. For the cell with the $n^+n^-p^+$ stack, the n^+ layer is in contact with Mo and the p^+ layer is in contact with ITO. According to literature reports, in the forward bias condition, the carrier lifetime at the Mo/p-type a-Si:H interface is longer than that at the transparent conductive oxide (TCO)/p-type interface.[51, 52] In other words, the carrier recombination rate in the former is lower than that in the latter. It was also reported that the ITO electrode usually forms ohmic contact with both p-type and n-type a-Si:H films.[53] However, after a high temperature annealing e.g., 300°C, the Shottky contact was formed between the ITO and the n-type a-Si:H, due to the formation of a thin interface oxide layer.[53] Therefore, the thermal history of the fabrication process of the solar cell can affect the contact properties and consequently the performance.

Nevertheless, from the dopant contamination of the i-layer point-of-view, both literature reports and our experimental result support that the Mo/$p^+p^-n^+$/ITO stack can provide better solar cell efficiency than the Mo/$n^+n^-p^+$/ITO can.

3.4 Deterioration of solar cell under electric stress vs. electric-light combined stress

Figure 16 shows the degradation of the $p^+p^-n^+$ cell under electric stress with and without being simultaneously illuminated with the solar light. The drop of the cell efficiency under the combined electric-light stress is larger than that under the electric stress alone. Therefore, the additional light illumination accelerates the cell degradation. According to Stutzmann,[54] the defect creation rate in an a-Si:H solar cell is determined by two opposite factors: defect generation vs. elimination, as shown in the following equation.

$$\frac{dN}{dt} = C_{sw} np - r_{ann} N \qquad [8]$$

where N is the density of dangling bonds, C_{sw} is the coefficient for defect creation rate, r_{ann} is the annealing rate for light- or thermal-induced recovery, n and p are electron and hole densities in the band tail states, respectively. The annealing term in Eq. 8 is associated with the recovery of the deteriorated cell, which is caused by the thermal effect from light illumination or electric stress.[43, 55] Under the simultaneous electric stress and light illumination, the defect generation rate is much faster than the thermal

annealing recovery rate,[43] i.e., the defect generation term in Eq. 8 is non-negligible. Under the light illumination condition, the defect creation in the a-Si:H solar cell is from the generation of electron-hole pairs.[22] The np product in the defect generation term of Eq. 8 corresponds to the probability of electron-hole recombination, which is proportional to the light illumination intensity,[54] i.e., it increases with the increase of the light intensity. It was reported that the electric stress is more effective in generating defects than the light illumination.[43] It was reported that the mechanism of defect generation in electric stress is the same as that in light illumination.[21] Since the np product in the former condition is larger than that in the latter condition, the former is responsible for the high defect generation rate. The combination of electric and light stresses is more effective in generating defects than that by electric stress or light illumination alone.

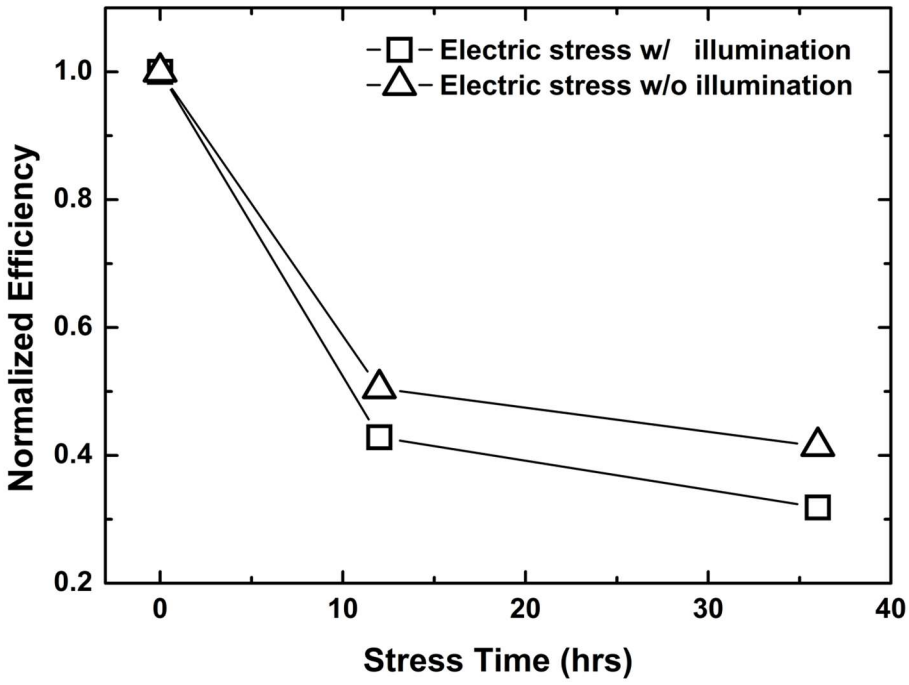

Figure 16. Stress time dependence of normalized efficiency ($p^+p^-n^+$ cell) on electric stress with and without light illumination.

3.5 Degradations of a-Si:H solar cells of different tri-layer deposition sequences under electric-light combined stress condition

Since the electric-light combined stress causes excessive damages to the solar cell, it would be interesting to understand the influence of the tri-layer stack structure on the deterioration mechanism. Figure 17 shows the time-dependent deterioration of power conversion efficiencies (PCE's) of solar cells with the $p^+p^-n^+$ and $n^+n^-p^+$ a-Si:H stacks. For the $p^+p^-n^+$ cell, the PCE drops drastically in the first 10 hrs, i.e., from 3.4% to 1.85%. Then, the drop of the PCE slows down, i.e., from 1.85% to 1.45% in the next 50 hrs. It saturates afterwards. Actually, the PCE of this cell decreases exponentially with the

increase of time, i.e., following the power law, as shown in the inset of Fig. 17, which is consistent with literature reports.[21, 43] The exponent of the curve in Fig. 17 is -0.16. It can vary with not only the stress condition but also the cell's property.[21, 43] The defect generation rates of different cells can be compared from their exponent numbers. For example, the exponent number of the cell under the electric stress condition is larger than that under the light illumination condition.[43] The exponential relationship between the cell deterioration and the stress time is related to the distribution of the band tail states in the p^- layer.[56, 57] The defect density saturates at around 10^{18} cm^{-3}, which is the density of deeply localized states in the valence band tail [55]. On the other hand, the degradation of the PCE of the $n^+n^-p^+$ cell is very different from that of the $p^+p^-n^+$ cell. It decreases very slowly with time, i.e., by 0.1% after 60 hrs. Other characteristics of the cell also deteriorate with the stress time following the same trends as that of the PCE. Figure 18(a) shows that the J_{SC} of the $p^+p^-n^+$ cell decreases exponentially with the stress time. For the $n^+n^-p^+$ cell, the J_{SC} decreases slowly with the stress time. The different deterioration behavior of those two types of cells may be originated from their i-layers. It was reported that under the forward bias condition, the carrier transport mechanism in the a-Si:H tri-layer is dependent on the electrical property of the i-layer.[48] The carrier transport in the $n^+n^-p^+$ cell is contributed by both the existing charges in the film and the current from the injection of major carriers. In the forward bias condition, without the disturbance of any external force, a semiconductor system tends to keep the thermal equilibrium state. In the intrinsic semiconductor layer, the relationship of $pn = n_i^2$, where n_i is the intrinsic carrier concentration, holds.[26] In the $n^+n^-p^+$ cell, when electrons

are injected from the Mo electrode to the n^+ layer, the thermal equilibrium state is broken because $pn > n_i^2$. In order to restore its thermal equilibrium state, part of the injected electrons have to recombine with holes as well as to diffuse to the n^- layer. At the same time, the thermal equilibrium of the p^+ layer is also broken because of the transfer of electrons from the p^+ layer to the ITO electrode. In this case, electrons in the electron-rich n^- layer move toward the p^+ layer to recombine with holes to restore the thermal equilibrium state. At the same time, the n^- layer is restored to the thermal equilibrium due to the injection of electrons from the n^+ layer. Consequently, the charge recombination process mainly takes place at around the p^+ layer. The defect generation in the n^- layer may be slow due to the slow carrier recombination, which results in the slow decrease of the J_{SC}. When the applied voltage is high, a large portion of electrons are transferred from the n^- layer toward the ITO electrode without being recombined with holes in the very thin p^+ layer. The injection current can be enhanced with the further increase of the applied voltage. For the $p^+p^-n^+$ cell, in contrast, when electrons are injected from the ITO electrode to the n^+ layer, the thermal equilibrium state of the n^+ layer is broken, i.e., $pn > n_i^2$. Some of the injected carriers recombine with minor carriers in the n^+ layer, i.e., holes. Those non-recombined electrons diffuse to the p^- layer. Since the p^- layer is hole-rich, the injected electrons are easily recombined with holes to restore the thermal equilibrium state. At the same time, the minority carriers, i.e., electrons, are transferred from the p^+ layer to the Mo electrode. The thermal equilibrium in the p^+ layer also collapses due to $pn > n_i^2$. Minority carriers of electrons in the p^- layer are transferred to the p^+ layer and subsequently recombine with holes to restore the

thermal equilibrium state. Consequently, the recombination process mainly occurs in the p^- layer. The carrier recombination efficiency in the p^- layer increases the defect generation rate. Therefore, the decrease of the J_{SC} in the $p^+p^-n^+$ cell is much faster than that in the $n^+n^-p^+$.

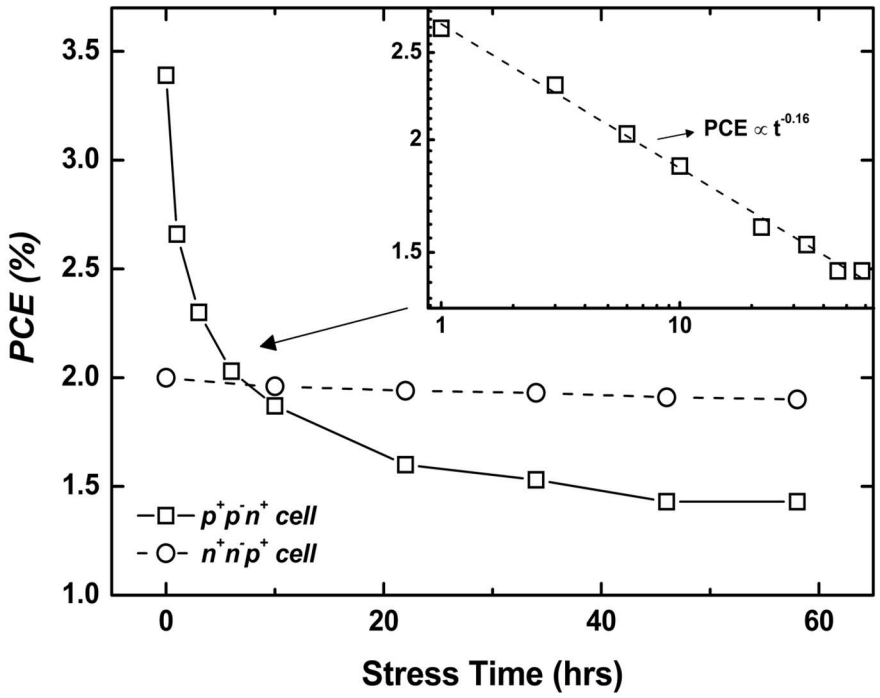

Figure 17. Variation of power conversion efficiency of solar cells with time under combined electric and light stress condition. Inset: power law dependence of PCE on stress time for $p^+p^-n^+$ cell.

Figure 18(b) shows the change of V_{OC} with the stress time in both the $p^+p^-n^+$ and $n^+n^-p^+$ cells. They can be correlated to curves in Fig. 18(a) because according to the following equation, V_{OC} and J_{SC} are related.[8]

$$V_{OC} = \frac{nkT}{q} \ln\left(\frac{J_{sc}}{J_0}\right) \quad [9]$$

where q is the electron charge, n is the ideality factor, k is the Boltzmann's constant, T is the absolute temperature, and J_0 is the dark saturation current.

Further on, the FF vs. stress time curve in Fig. 18(c) can be related to curves in Fig. 18(a) and (b) according to the following equation.[8]

$$FF = \frac{P_{\max}}{V_{OC} \times J_{SC}} \quad [10]$$

where P_{max} is the maximum output power of a solar cell.

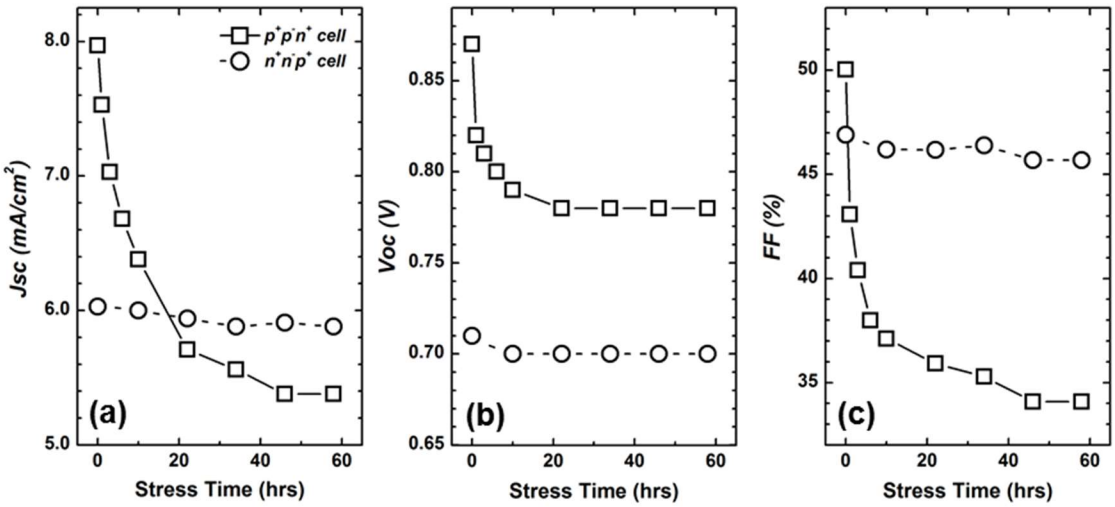

Figure 18. Changes of (a) J_{SC}, (b) V_{OC}, and (c) FF of $p^+p^-n^+$ and $n^+n^-p^+$ a-Si:H solar cells with time under combined current-illumination stress.

It is well-known that the series resistance (R_s) and the shunt resistance (R_{sh}) of a solar cell are affected by the bulk resistance and current leakage through the a-Si:H stack.[38] They both change with the light illumination. The defect generation from the voltage stress increases not only the bulk resistance but also the leakage current, i.e., increasing the R_s and decreasing the R_{sh}. Consequently, the photocurrent decreases with the increase of the defect density in the cell. Figure 19 shows changes of the R_s and R_{sh} with the stress time of (a) $n^+n^-p^+$ cell and (b) $p^+p^-n^+$ cells. They were estimated from the inverse slope of the current-voltage (I-V) characteristic at V_{OC} and I_{SC}, respectively. Changes of both resistances with the stress time are consistent with those of the PCE, V_{OC}, J_{SC}, and FF in Figs. 17 and 18. Since the defect generation rate in the $n^+n^-p^+$ cell under the combined electric-light stress condition is much slower than that in the $p^+p^-n^+$ cell, the photocurrent in the former decreases at a slower rate than that in the latter. For

the $n^+n^-p^+$ cell, therefore, the R_s increases and the R_{sh} decreases slowly, as shown in Fig. 19(a). For the $p^+p^-n^+$ cell, since the defect generation rate increases exponentially with the stress time, the leakage current decreases exponentially accordingly. Therefore, the corresponding R_s increases and R_{sh} decreases exponentially with the stress time, as shown in Fig. 19(b).

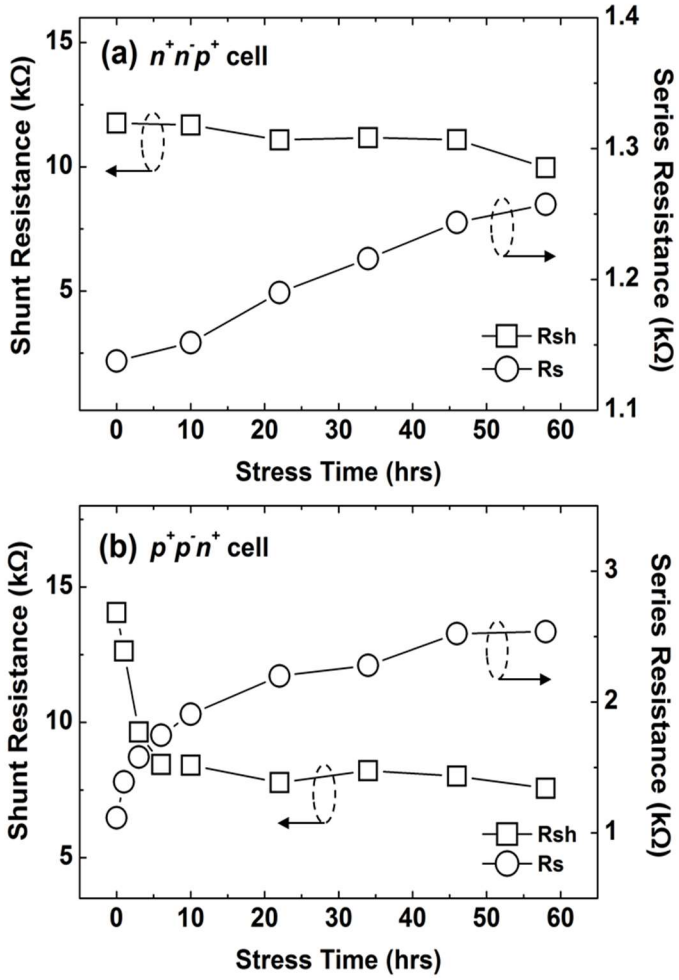

Figure 19. Changes of shunt and series resistances of (a) $n^+n^-p^+$ and (b) $p^+p^-n^+$ a-Si:H solar cells with time under combined electric-light (5V and AM 1.5G) stress.

3.6 Recovery of degraded solar cell

Previously, it was reported that the process induced defects in the a-Si:H device could be removed with a thermal annealing step.[58] Figure 20 shows the (a) V_{OC}, (b) J_{SC}, (c) FF, and (d) PCE vs. time curves of solar cells after they were stressed with the combined electric-light stress for 60 hrs at room temperature followed by 200°C annealing. The degraded $n^+n^-p^+$ cell was restored to its original state in less than 1 hour. However, for the degraded $p^+p^-n^+$ cell, all device characters were only partially recovered even after 4 hours of annealing. It was reported that a-Si:H solar cells damaged by the prolonged light illumination or low-voltage stress could be restored to their initial states after 10-100 min of annealing at 130-200°C.[14, 21, 24] Since the defect generation mechanism in the light illumination condition is the same as that in the electric stress condition, defects generated by the combined electric-light stress should be easily removed with a thermal annealing step. However, Fig. 20 shows that the a-Si:H tri-layer deposition sequence is an important factor affecting the damage repair process. Defects in the a-Si:H film are often in the dangling bond form due to the loss of the passivation H atoms.[11, 58, 59] Those H atoms are still around the defect sites and can be easily attached to them upon a thermal annealing step.[58] For the $p^+p^-n^+$ solar cell, the defect generation process is more complicated. For example, Fig. 20(a) shows that its V_{OC} was improved from 0.77V to 0.84V after 5 hours of annealing. It may be that B dopants in the p^- layer were partially deactivated during the combined electric-light stress, which degraded the p^-n^+ junction. Compared with P dopants, B dopants in the Si network generate more serious strains.[60] When H atoms in the film are attached to the B

dopant to release the strain, e.g., by forming B^-H^+ pair, the dopant function is lost.[60-62] When a higher annealing temperature, e.g., > 200°C, is applied, the deactivated dopant may be more effectively restored. It was reported that B dopants can be activated when annealed at temperatures greater than 200°C.[63, 64]. The partially restored $p^+p^-n^+$ solar cell in this study was further annealed at 230°C for an hour. After the additional annealing, the V_{OC} returned into the initial value, i.e., from 0.84V to 0.87V as shown in Fig. 20(a). At the same time, other parameters, i.e., J_{SC}, FF, and PCE are also restored close to the initial values, as shown in Fig. 20(b), 20(c), and 20(d).

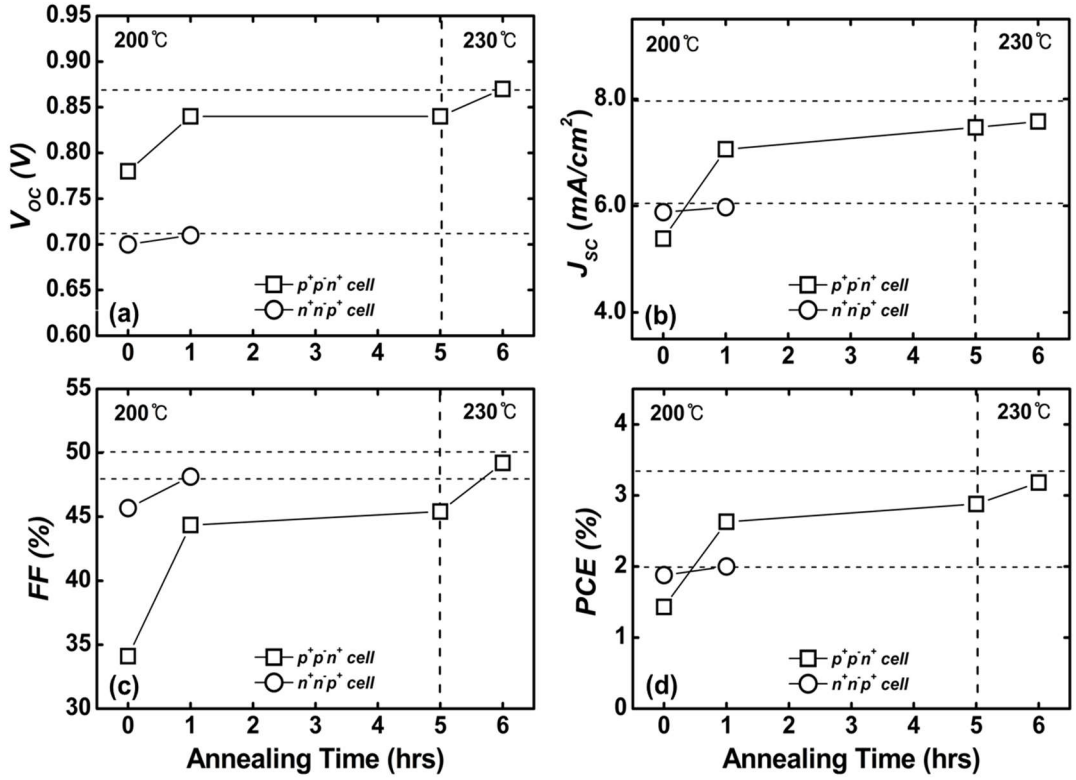

Figure 20. Changes of (a) V_{OC}, (b) J_{SC}, (c) FF, and (d) PCE of $p^+p^-n^+$ and $n^+n^-p^+$ a-Si:H solar cells with annealing time at 200°C. Devices was previously stressed for 60 hours under combined electric-light (5V and AM 1.5G) stress.

3.7 Summary

The pin and nip a-Si:H solar cell were prepared by PECVD in the same chamber using the one pump down process. The electrical property of the i-layer is affected by the deposition condition of the previous film. The $p^+p^-n^+$ or $n^+n^-p^+$ stack rather than the pin or nip stack are formed. The overall performance of the $p^+p^-n^+$ cell was better than that of the $n^+n^-p^+$ cell due to the suppression of defect generation related to the injection current. In comparison with the electric stress alone, the combined electric-light stress accelerated the cell degradation because the increase of defect generation. The degradation of the $p^+p^-n^+$ cell was more serious than that of the $n^+n^-p^+$ cell since the recombination of charge carriers is stronger in the p^- layer than in the n^- layer. In the $p^+p^-n^+$ cell, the PCE degradation with time follows the power law relationship with an exponent constant of -0.16. The degraded $n^+n^-p^+$ cell was completely restored to its initial state after an hour of 200°C annealing. However, the degraded $p^+p^-n^+$ cell was partially restored even after additional 4 hours annealing. The cell was almost completely restored with the further annealing at 230°C for an hour. The B dopants were reactivated Mo/$p^+p^-n^+$/ITO structure after the high temperature annealing. In summary, the deposition sequence of the a-Si:H tri-layer influenced the material and electrical properties of the i-layer, which affects the solar cell performance, deterioration process, and recovery efficiency.

CHAPTER IV

WAVELENGTH AND POWER DENSITY EFFECTS ON LIGHT SENSING OF A-SI:H PIN DIODE[2]

4.1 Introduction and motivation

The hydrogenated amorphous silicon (a-Si:H) semiconductor was first reported by Chittick and his colleagues in 1969.[65] In 1975, Spear and LeComber demonstrated that the a-Si:H film could be doped with phosphorus (P) or boron (B) with the PECVD method.[16] Since then, a-Si:H thin films have been widely used in many electronic and optoelectronic devices, such as thin film transistors (TFTs), photodiodes, and image sensors.[13, 66, 67] Also, a-Si:H pin diodes have been used as optical signal detectors in optocoupler systems as well as solar cells for energy harvesting.[49, 68-70] Since the a-Si:H film has high sensitivity to visible light, many of these applications are in the 400 nm to near-IR range. For the best device performance, it is necessary to achieve a high light-to-electricity conversion efficiency. Many methods have been used to obtain the high efficiency, such as the graded interface structure, optimized fabrication process, surface plasmonic enhancement effect, and photochemical upconversion.[71-74] For the device characterization, the pin diodes are often characterized under the broad band light illumination condition, e.g., a solar simulator at AM 1.5G. In practice, however, they are exposed to lights of diverse wavelengths and power densities. The photo responsibility

[2] Data reported in this chapter is partially reproduced from "Light Sensing of pin Diode – Wavelength and Intensity Effects", by Kibum Kim and Yue Kuo, published by ECS Transaction, 72(3), pp. 15-20 (2016), and by permission of ECS.

of the a-Si:H diode is sensitive to the wavelength and power density of the light.[75-77] Also, the light-sensing of the pin diode on those factors was rarely studied. In this chapter, the electrical and optical responses of the a-Si:H pin diode under the illumination of 3 narrow band LED lights, i.e., red, green, and blue will be studied.

4.2 Experimental

Figure 21 shows the a-Si:H diode structure and light measurement setup. The a-Si:H pin tri-layer was deposited by PECVD (Applied Materials, AMP Plasma I, 50 kHz) in one pump-down within the same chamber at 260°C. Table 3 lists deposition conditions of individual films. In order to minimize the cross-contamination of the dopant, after the deposition of a film, the chamber was purged twice with Ar and subsequently evacuated to a high vacuum. The 80 nm thick ITO top and bottom electrodes were deposited by the same sputtering process. The top ITO film was wet etched into 2 mm diameter dots as the top electrodes. The transparent electrodes were used in this study for the easy detection of the light transmittance through the pin tri-layer stack. The complete diode was annealed at 200°C for 30 min in air before the device characterization. Separately, in order to study the light reflection effect, an Ag coated glass was placed underneath the bottom ITO electrode. Since Ag reflects over 95% of the visible light,[78] the incident light transmitted through the complete diode will be reflected from the Ag surface back to the pin stack, which enhances the light-to-electricity conversion efficiency.

The diode was illuminated with the light from the top electrode side. Commercial Thorlabs red (625 nm, M625L3), green (530 nm, M530L3), and blue (470 nm, M470L3) LEDs with various light power densities, i.e., 0.705, 1.411, 2.822, 4.232, or 5.643 mW/cm^2, were used as the illumination light sources. As shown in Fig. 21, the light transmitted through the diode with ITO electrodes was measured with a digital power meter (PM100A, Thorlabs).

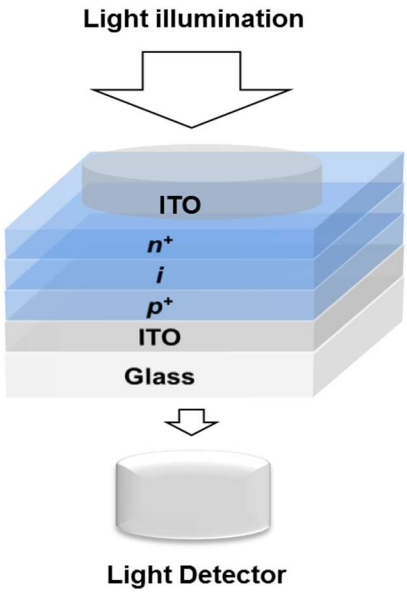

Figure 21. a-Si:H pin diode structure and experimental setup.

TABLE 3. Deposition conditions of a-Si:H pin diode

Film thickness	Gas flow rate (sccm)				Power (W)	Pressure (mTorr)
	SiH_4	H_2	B_2H_6	PH_3		
p^+ 15nm	35	400	20	0	150	700
i 300nm	50	200	0	0	500	500
n^+ 20nm	60	1000	0	20	500	700

4.3 Wavelength effect on EQE

Figure 22 shows EQEs of the a-Si:H pin diode illuminated under different lights at various power densities. The EQE was calculated from the equation of [8]

$$\frac{SR(\lambda) \cdot E(\lambda)}{q} = EQE(\lambda) \qquad [11]$$

where SR(λ) is the spectral response, i.e., the ratio of the short-circuit current density (J_{SC}) to the incident light power density, q is the charge of the electron, and E(λ) is the energy of the incident photon. Fig. 22 shows that the highest efficiency is obtained under the medium wavelength green light illumination condition, which is consistent with literature reports.[3, 12, 79] In general, the EQE of a diode is mainly contributed by three factors: (i) the parasitic light absorption, i.e., from the n^+ or p^+ layer,[80] (ii) the loss of incident light from reflection, etc., and (iii) the recombination of photo-generated

carriers.[8] The first two factors do not contribute to the generation of charge carriers in the device. For the Fig. 21 set up, the incident light passes through the tri-layer in the order of n^+, i, and p^+ layers. Since light absorbed by the n^+ layer does not contribute to the photocurrent generation, the diode's efficiency decreases with the increase of its thickness. It was reported that the light transmittance through the un-doped a-Si:H layer increases with the increase of the wavelength.[76] Since the blue light has the shortest wavelength among the three lights, it is more absorbed by the n^+ layer than the other two lights are. Therefore, the EQE of the cell under the blue light illumination can be lower than those of the other two lights. On the other hand, a larger portion of the longest wavelength red light can reach and be absorbed by the i-layer. However, since the energy of the light is inversely proportional to the wavelength,[8] the red light is less effective in generating charge carriers than the blue or green light is. From the combination of the loss of the incident light in the n^+ layer and the effectiveness of generating charge carriers, the medium wavelength green light contributes to a higher EQE than the other two lights do.

The carrier recombination loss can be a serious factor for the low EQE. Photo-generated electrons and holes in the i-layer migrate toward opposite electrodes where they are collected. Some of these charge carriers may recombine before reaching the electrode, which causes the loss of the photocurrent. This phenomenon is especially obvious under the illumination of the short wavelength light. It was reported that under the short wavelength light illumination, the photo-generated carriers at near the interface close to light source, i.e., the n^+/i interface in the Fig. 21 device, can diffuse against the

internal electric field.[8, 81, 82] Since the short wavelength light has a shallow penetration depth, a large portion of the incident light is absorbed around the n^+/i interface. Then, the back-diffusing and recombination of the photo-generated charge carriers occur shortly upon their generations. This can be another factor for the low EQE of the blue light illuminated diode.

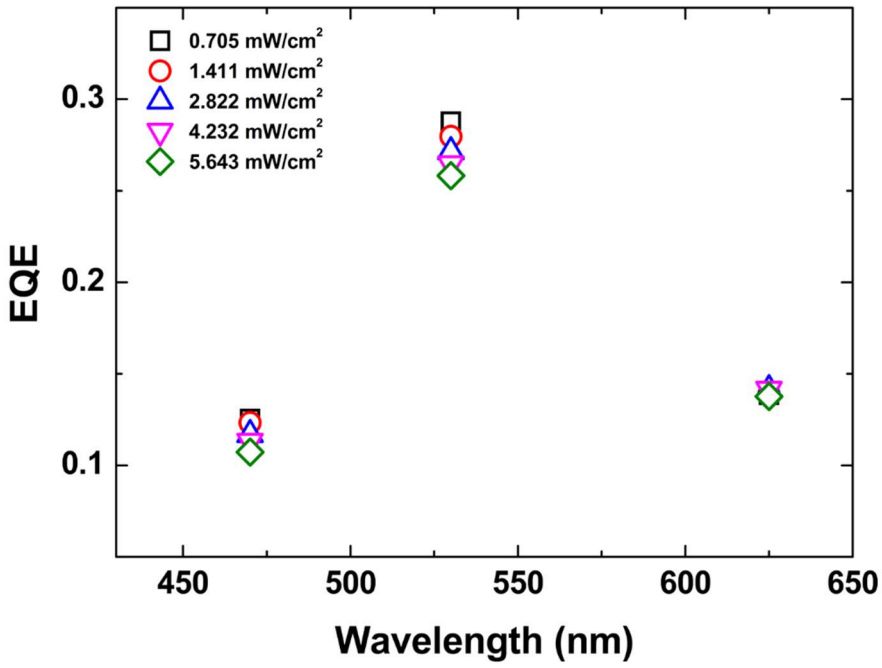

Figure 22. EQE dependence on light wavelength and power intensity.

4.4 Light intensity effect on EQE

Figure 23 shows the diode's EQE dependence on the illumination light density, which is redrawn from data of Fig. 22. The EQE is almost independent of the power

density of the red light, but it decreases with the increase of the power density for both blue and green lights. According to Eq. 11, the EQE is a reference of the spectral response of the diode, i.e., the ratio of the J_{SC} to the incident light power density. The Fig. 23 result can be further interpreted by correlating the change of the J_{SC} to the incident light power density. Figure 24 shows the dependence of the J_{SC} on the light power density under the (a) red, (b) green, and (c) blue light illumination conditions. Assuming that the loss of the photo-generated current from the carrier recombination is negligible, the expected J_{SC} should be proportional to the incident light power density. In Fig. 24(a), under the red light illumination, the experimental data almost coincide with the expected date, i.e., without the carrier recombination. However, Fig. 24(b) and 24(c) show that under the green and blue light illumination conditions, the experimental data are different from the expected data and the difference increases with the increase of the light power density. Therefore, under the short wavelength light exposure condition, the carrier recombination phenomena cannot be neglected. The more charge carriers are generated, the more serious the change recombination phenomenon is.

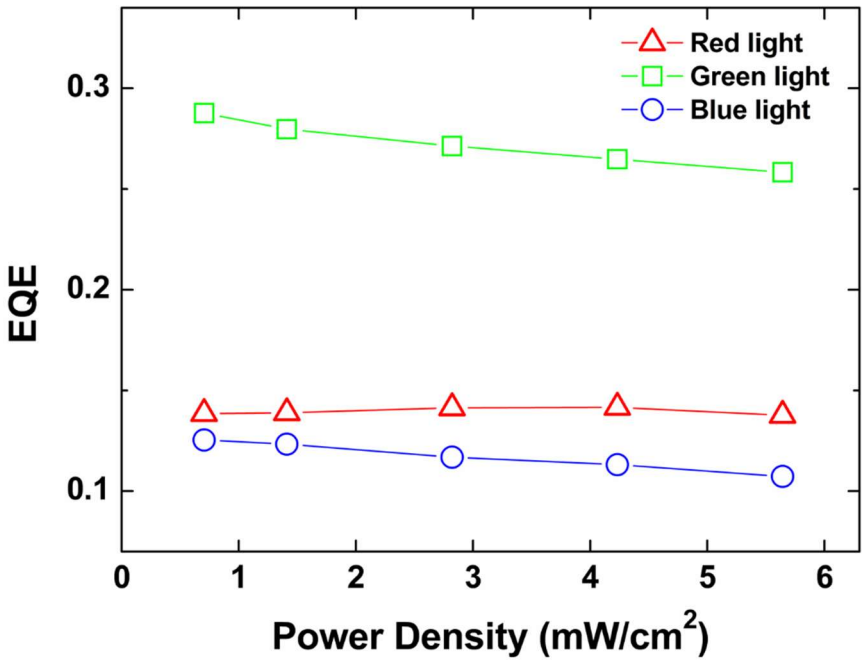

Figure 23. Change of EQE with the illumination light power density of different lights.

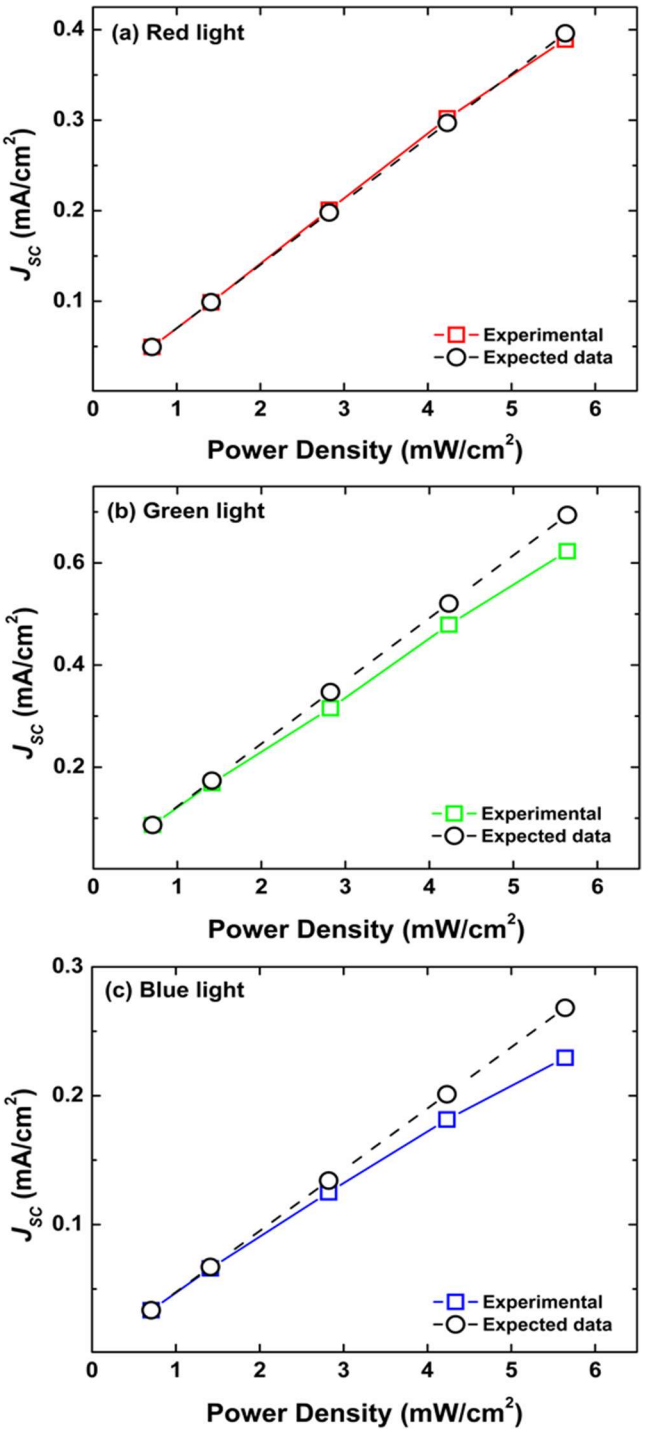

Figure 24. Dependence of photo-current density on power densities of (a) red, (b) green, and (c) blue light illumination.

Previously, it was stated that the light absorption through the pin tri-layer could be an important factor for the light-to-electricity conversion efficiency. In order to verify this effect, light absorptions through the n^+, n^+/i, and n^+/i/p^+ layer were measured with respect to the power density, as shown in Figure 25(a), (b), and (c). According to the Beer's law,[83] the attenuated light intensity I is related to the incident light intensity I_O and the film thickness x as shown below:

$$I = I_O e^{-a \bullet x} \qquad [12]$$

where a is the absorption coefficient. For the same film with equivalent thickness, the I/I_O ratio should be constant and independent of the power density of the incident light. Curves in Fig. 25 confirm that the light penetration depth is dependent on the wavelength. In Figs. 25(a) and (b), about 79% of the incident blue light was absorbed by the n^+ layer and about 99% of the light was absorbed by the i/n^+ stack. It is also consistent with the explanation of the low diode EQE under the blue light illumination condition in Fig. 22, i.e., the majority of the incident light was absorbed by the n^+ layer. Also, photo-generated electrons and holes were lost near the i/n^+ interface. In contrast to the travel of electrons to the n^+ layer, holes had to travel a long distance to reach the p^+ layer.[42] The chance for holes to be trapped by defect in the i-layer is high, which causes the one-sided recombination of the holes. The imbalance of the carrier collection can cause the decrease of the photocurrent with the increase of the power density of the blue light, which was observed in Fig. 24. The same trend was observed under the green light

illumination condition. However, since the green light was less absorbed by the n^+ layer than the blue light was, i.e., 70% vs. 79%, the former generated more electrons and holes and had less one-sided recombination of the holes than the latter. Therefore, the green light caused the higher diode EQE than the blue light did. On the other hand, about 54%, 65%, and 76% of the incident red light were absorbed by the n^+, n^+/i, and n^+/i/p^+ layers, separately. This indicates that in spite of the low energy, a large portion of the red light could penetrate through the whole n^+/i/p^+ layers. The one-sided recombination of holes generated near the n^+/i region is minimum, which suppresses the imbalanced carrier collection. Therefore, under the red light illumination condition, the EQE is almost independent of the power density. The light absorption mechanism could explain the wavelength effect on the EQE and the loss of the photocurrent in the a-Si:H pin diode.

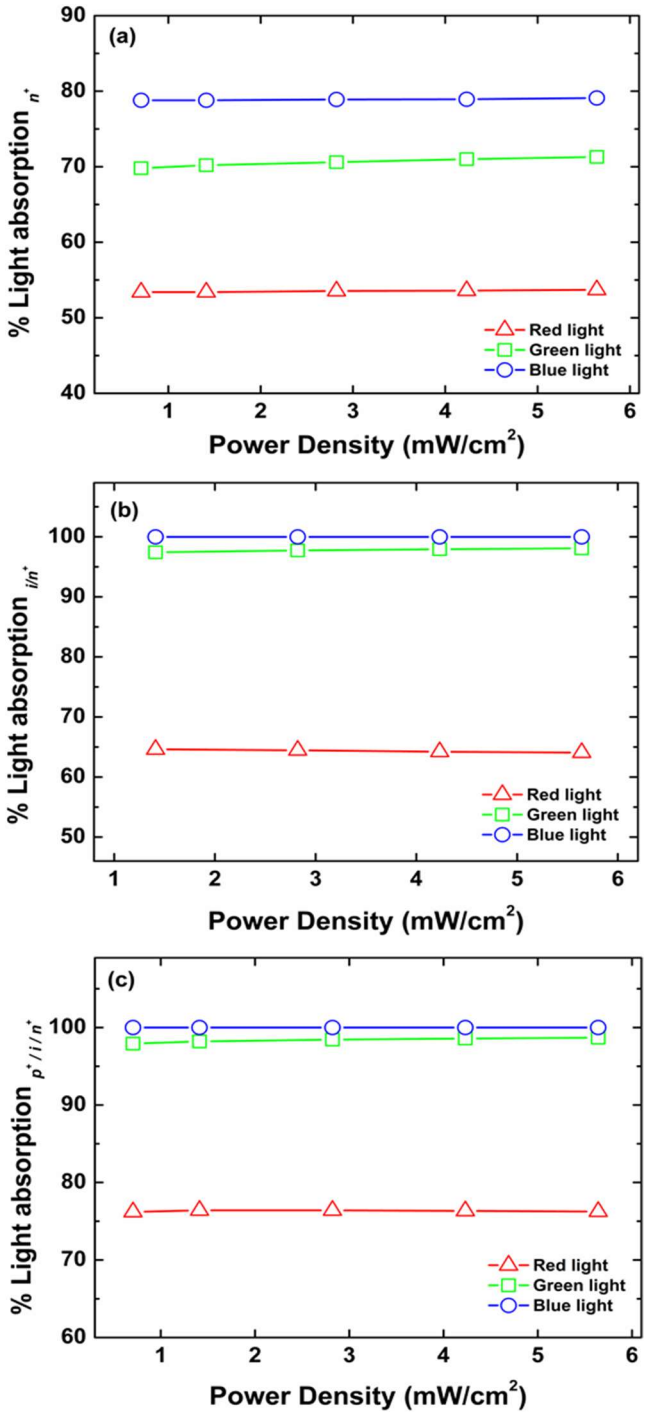

Figure 25. Light absorptions of (a) n^+, (b) i/n^+, and (c) p^+in^+ layers of red, green, and blue incident lights at various power densities.

4.5 Light wavelength and power intensity effects on diode characteristics

Changes of internal resistances of the diode, i.e., series resistance (R_S) and shunt resistance (R_{sh}), reflect the efficiency in converting light to electricity. They are usually estimated from the current vs. voltage, i.e., I-V, curve. For example, R_S is the inverse slope of curve at I = 0 A and R_{sh} is the inverse slope of the curve at V = 0 V. Figure 26 shows I-V curves under (a) red, (b) green, and (c) blue light illuminations at various power densities. It is clear that under the same light illumination, the V_{OC} increases slightly but the short circuit current I_{SC} increases drastically with the increase of the power density. Slopes of the curve at the V_{OC} and I_{SC} also vary with the increase of the light power density. Figure 27 shows the power density effect on the (a) R_S and (b) R_{sh}, separately. In Fig. 27(a), the R_S decreases linearly with the increase of the power density independent of the wavelength. According to the literature report,[38] R_S represents the photocurrent flowing across the diode, which decreases with the increase of the light intensity. The magnitude of the R_S is related to the wavelength of the illumination light. The order of R_S' under different light illuminations can be estimated from Fig. 24, i.e., the green light generates the largest photocurrent and the blue light generates the lowest current. On the other hand, the R_{sh} represents the leakage current through the diode, which is contributed by factors such as defects, impurities, or the cell edge.[38] A very large R_{sh} is preferred for a high performance photodiode. In general, the leakage current increases with the increase of the photocurrent, i.e., R_{sh} is proportional to R_S. Fig. 27(b) shows that the R_{sh} decreases with the increase of the light power density just like that in Fig. 27(a). However, the magnitude of the R_{sh} is in the order of red, blue, and green,

which is different from that of R_S. The discrepancy can be explained by the loss of photo-generated holes. As discussed previously, holes generated by the blue light are subject to the easy recombination near the n^+/i interface region while the recombination of holes under the red light illumination occurs evenly across the i-layer. The unbalanced carrier recombination under the blue light illumination is the cause of its high current leakage and low R_{sh}.

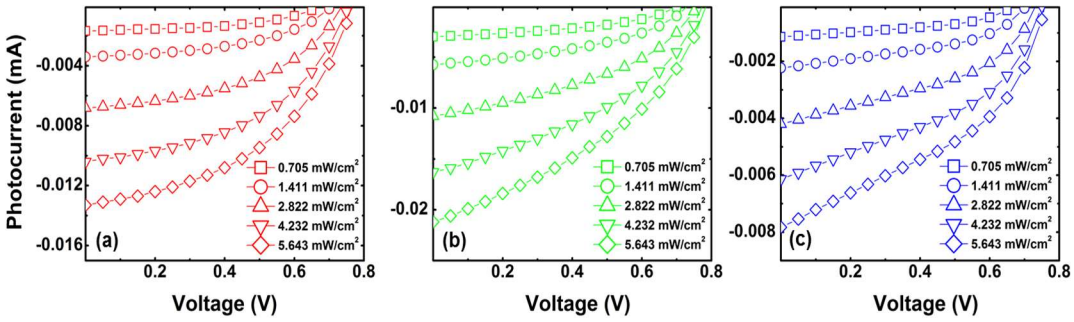

Figure 26. I-V curves of a-Si:H pin diode under the illumination of (a) red, (b) green, and (c) blue lights at various light intensities.

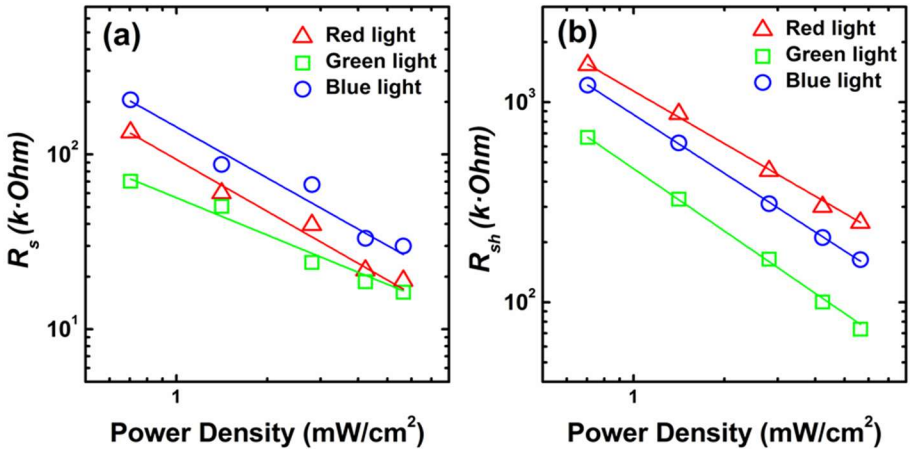

Figure 27. Changes of (a) R_S and (b) R_{sh} with the illumination light power density under red, green, and blue light illumination conditions.

Figure 28 shows the relationship between J_{SC} and V_{OC} under red, green, and blue light illumination conditions. According to a literature report,[84] the relationship between J_{SC} and V_{OC} in a solar cell can be expressed by the equation of:

$$J_{SC} = J_{SO} \exp[eV_{OC}/(nkT)] \quad [13]$$

where J_{S0} is the saturation current in dark, e is the electron charge, n is the ideality factor, k is the Boltzmann's constant, and T is the absolute temperature. In Fig. 28, the Eq. 13 relationship is held for red, green, blue lights. The n value is determined by the density of recombination centers in the depletion region.[85] For an ideal device without any recombination center, n is 1. In the real device, since defects and impurities cannot be eliminated, n is greater than 1. All curves in Fig. 28 have similar n values, i.e., 1.58, 1.51,

and 1.59 for the red, green, and blue lights, respectively, which is within the literature report range of 1.4 - 1.6.[86, 87] Therefore, the density of recombination centers in the tested device is independent of the wavelength of the illumination light.

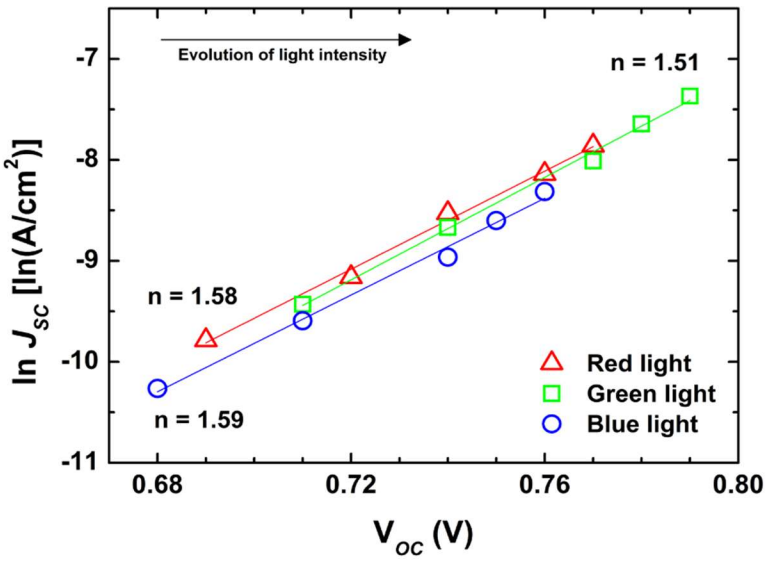

Figure 28. Relationship between short circuit current density (J_{SC}) and open circuit voltage (V_{OC}) of a-Si:H diode on the increase of light intensity.

4.6 Back reflector effect

When the unabsorbed light is reflected from the bottom electrode back to the pin tri-layer for further absorption, the photon-to-electricity conversion efficiency can be enhanced. Since the penetration depth of the light depends on the wavelength, the enhancement of the efficiency is sensitive to the wavelength. Figure 29 shows the effect of the Ag reflector on the EQE under the (a) red, (b) green, and (c) blue light illumination conditions, separately. Under the red light illumination, i.e., Fig. 29(a), the EQE is increased by the same amount independent of the light power density. As shown in Fig. 25(c), due to its long wavelength, only 75% of the red light was absorbed by the pin tri-layer. The unabsorbed light is reflected by the Ag reflector to enhance the EQE. Also, since the light absorption ratio is independent of the power density, the enhancement is unchanged. On the other hand, the green and blue illumination lights are completely absorbed by the pin tri-layer, no light is reflected by the bottom reflector to enhance the EQE.

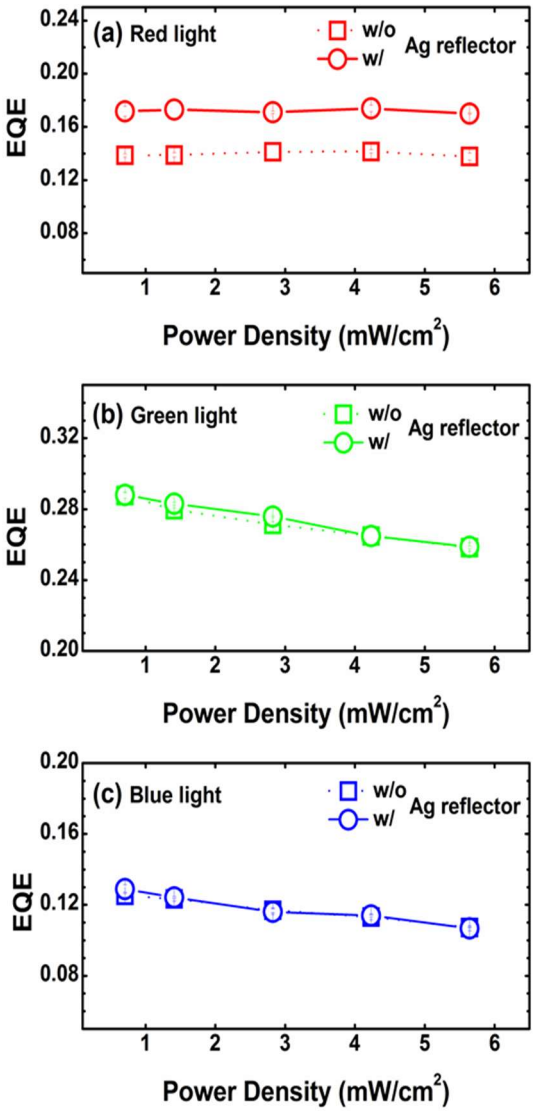

Figure 29. Effect of Ag reflector on EQE at different light power densities of (a) red, (b) green, and (c) blue LED.

4.7 Summary

The light sensing of the a-Si:H pin diode under different illumination lights at various power densities has been studied. The EQE is dependent on the light absorption efficiency through the tri-layer stack and the band energy of the light. When the power

density of the green and blue lights was increased, the EQE decreased owing to the increase of the recombination of photo-generated holes during transferring to electrodes. With the increase of the illumination light power, both R_S and R_{sh} decreased linearly. Although the blue light generates less photocurrent than the red illumination light does, the former's R_{sh} is lower than that of the latter. This phenomenon can be explained by the former's low collection efficiency of photo-generated holes. Both the J_{SC} and the V_{OC} of the diode increased with the illumination light power density independent of the wavelength. They can be correlated exponentially similar to the solar light illumination condition. The addition of an Ag back reflector only enhanced the EQE under the red light illumination condition because the long wavelength light is not totally absorbed by the pin tri-layer. In summary, the light sensing of the a-Si:H pin diode is dependent on the complicated mechanism of generation, transfer, and recombination of charge carriers in the pin tri-layer.

CHAPTER V

EFFECT OF INTRINSIC LAYER DEFECT DENSITY ON LIGHT SENSING PERFORMANCE OF A-SI:H PIN DIODE[3]

5.1 Introduction and motivation

The hydrogenated amorphous silicon (a-Si:H) contains a large number of defects and is subject to structure change under stressed condition.[13] For example, when illuminated for a long period of time, it suffers from the Staebler-Wronski effect (SWE) due to the creation of metastable defects in the a-Si:H network.[14] Those defects are dangling bonds generated from the breakage of weak Si-Si or Si-H bond and the migration of hydrogen (H) atoms during the non-radiative recombination process of photo-generated electron-hole pairs.[22]

Since the a-Si:H pin diode is very effective in harvesting lights in the visible wavelength range, it is often used as the optical detector or solar cell.[49, 68-70] The major concern of this kind of devices is the stability of the composing materials. Normally, the stability of the a-Si:H diode is studied by exposing it to the light for a long period of time.[39, 40, 42] However, it takes a long time to get the result because the photon energy is limited. There are a report of studying the stability of the device using an electric bias stress method.[21] It appears that the electric bias stress can generate the same defects as

---

[3] Data reported in this chapter is partially reproduced from "Light Sensing of a-Si:H pin Diode – Mechanism of Asymmetric Charge Carrier Transfer", by Kibum Kim and Yue Kuo, published by IEEE Sensors Letters, 1(1), ASN: 3500304 (2017), and by permission of IEEE.

the light exposure stress.[21] Since the stress voltage can be easily controlled to simulate the harsh environment, the test time can be shortened. Furthermore, the electric bias stress can be used in combination with the light exposure.[43, 88] More detailed information on the deterioration of the a-Si:H diode can be obtained within a short period of time.

The light sensitivity of the a-Si:H pin diode is largely affected by defects within the intrinsic (i) a-Si:H layer and wavelengths of the illumination light.[18, 43, 76, 79, 89] Regarding this kind of factors, one possible concern of the diode could be the asymmetric loss of photo-generated carriers.[90] Normally, it originates from long carrier transfer distances caused by short wavelength lights. Since the i-layer is responsible for the carrier transport, its thickness could be another consideration affecting the carrier transfer distance. In this chapter, the effect of the i-layer thickness on the light sensitivity of a-Si:H pin diodes under different wavelength illumination lights will be studied.

5.2 Experimental

Figure 30 shows the structure of the a-Si:H pin diode used in this study. The a-Si:H p^+ (15 nm)/i (200 or 300 nm)/n^+ (15 nm) tri-layer was deposited on a Mo (200 nm-thick) Corning 1737 glass by PECVD (Applied Materials, AMP Plasma I, 50 kHz) within the same chamber in one pump-down at 260°C. The deposition power was controlled from the RF power generator with an automatic matching network. Deposition conditions of the individual pin layer are summarized in Table 4. For the top electrode, 80 nm-thick ITO was sputtered on top of the pin tri-layer, followed by wet-etch into 2 mm diameter electrodes. The complete diode was annealed at 200°C for 30 min in air.

The a-Si:H pin diode was characterized by applying a voltage from -2 to 2V (on the bottom Mo electrode) and simultaneously illumination (through the top ITO electrode side) with a red (625 nm), green (530 nm), or blue (470 nm) LED made by Thorlab. The power density on the diode was fixed at 2.822mW/cm^2. For the defect generation within the i-layer, a combined stress technique composed of the AM 1.5G solar light (Solar Light Co., Model: 16S-300-002) and 5V was used.

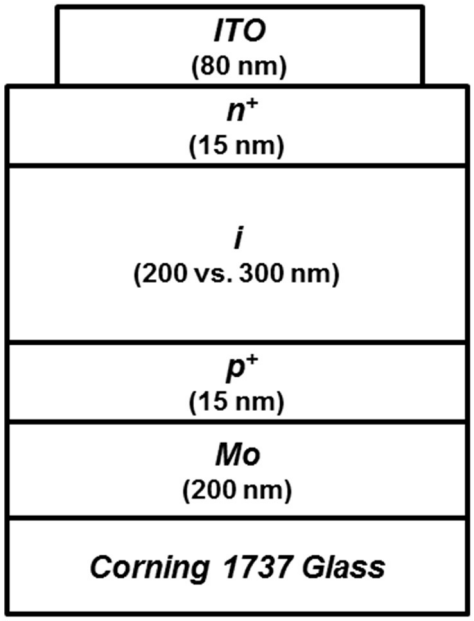

Figure 30. a-Si:H pin diode structure.

TABLE 4. Deposition conditions of a-Si:H pin diode

Film thickness	Gas flow rate (sccm)				Power (W)	Pressure (mTorr)
	SiH_4	H_2	B_2H_6	PH_3		
p^+	35	400	20	0	150	700
i	50	200	0	0	500	500
n^+	60	1000	0	20	500	700

5.3 Intrinsic layer thickness effect

Figure 31 shows the current density (J) - voltage (V) curves of a-Si:H pin diodes with (a) 300 and (b) 200 nm i-layer, separately, under red, green, and blue light illuminations. For the 300 nm-thick i-layer diode in Fig. 31(a), J-V curves of the red and green light illumination conditions show typical behavior, i.e., a low resistance at the open circuit voltage (V_{OC}) and a very large resistance at the short circuit current density (J_{SC}). However, under the blue light illumination, the J-V curve deviates from the normal behavior, i.e., a relatively large resistance at V_{OC} and a small resistance at J_{SC}. For the 200-nm thick i-layer diode in Fig. 31(b), the J-V curves show the normal behavior independent of the wavelength of the illumination light.

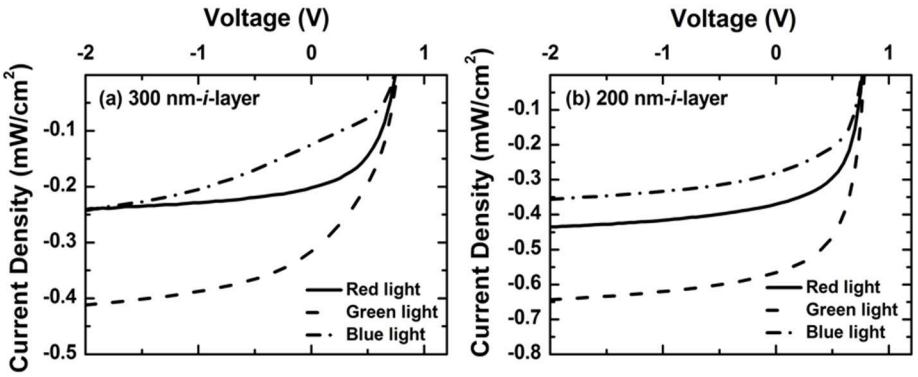

Figure 31. J-V characteristics of the a-Si:H photodiode with (a) 300 and (b) 200 nm i-layer under red, green, and blue light illuminations.[91]

Figure 32 shows the dependence of current density drop rate and the external quantum efficiency (EQE) on the wavelength of the illumination light, which were calculated from Fig. 31(a) and (b) data. The current density drop rate was estimated by the ratio of the J_{SC} at 0V to the current density at -2V. The EQE was calculated from Eq.11. Figure 32 shows that the current density drop rate decreases with the decrease of the i-layer thickness under all illumination lights. Also, the change of the current density drop rate decreased with the increase of the wavelength of the light, i.e., 30% at 470 nm, 12% at 530 nm, and 1% at 625 nm. Since the photo-generated current density is largely affected by the leakage current in the diode,[21, 43, 88] the quality of the i-layer, e.g., defects, must play on important role in the diode performance. The increase of the i-layer thickness corresponds to the increase of the defects in the i-layer. The result of Fig. 32 indicates that the leakage current is more dominated by the i-layer thickness than the wavelength of the light. Fig. 32 also shows that the EQE increases with the decrease of the i-layer thickness under all illumination lights. However, the dependence of EQE to

the wavelength is not monotonic, i.e., the green light generates a higher EQE than the blue or red light does. The similar result has been supported in the literatures.[3, 12, 79] Here, there is a discrepancy between the influence of the i-layer to the current density drop and the EQE. For example, when the i-layer thickness is reduced from 300 nm to 200 nm, the current density drop rate decrease is the largest under the blue light illumination. However, the EQE increase is the smallest under the blue light illumination. Based on Eq. 11, this phenomenon could appear when, at the constant light power density, the J_{SC} to the incident light energy is still low even after the decrease of the i-layer thickness.

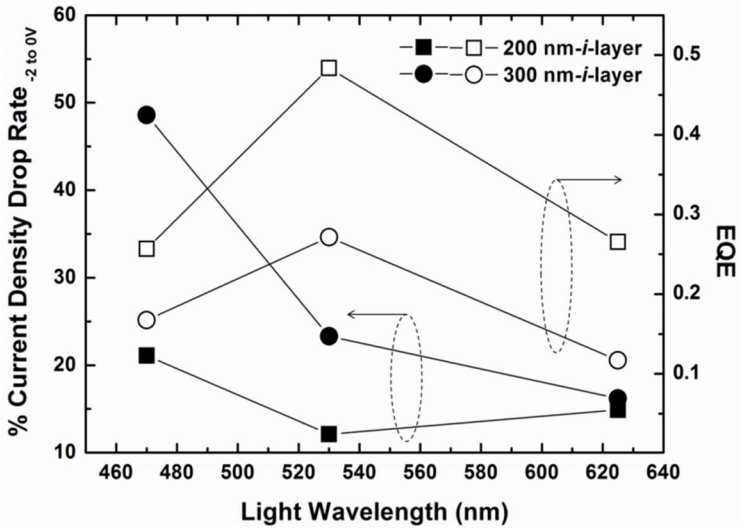

Figure 32. Dependence of current density drop rate and EQ*E* on red, green, and blue light illuminations.[91]

5.4 Carrier loss mechanism

Figure 33 shows the band diagram of the a-Si:H pin diodes with (a) 300 and (b) 200nm thick i-layer under the negative voltage and blue light illumination. According to our previous study,[90] the blue light has the highest energy among the three illumination lights. The incident blue light is almost totally absorbed at the closer vicinity of the i/n^+ interface. Therefore, the photo-generated electrons near the interface are effectively collected by the top ITO electrode due to the short traveling distance. At the same time, the photo-generated holes have to travel a relative long distance to reach the bottom Mo electrode.[92] Furthermore, the lifetime of the hole in the a-Si:H material is much shorter than that of the electron.[8, 93, 94] Therefore, the probability for losing holes in the device is higher than that for losing electrons.[42]

Since the i-layer in Fig. 33(a) is 100 nm thicker than that in Fig. 33(b), i.e., 300 vs. 200 nm, the blue light generated holes in the former have to travel a longer distance to reach the bottom Mo electrode than those in the latter. The loss of holes in the former is more serious than that in the latter. Therefore, the asymmetric transfer of electrons and holes in the diode with a thicker i-layer is more serious than that with a thin i-layer.

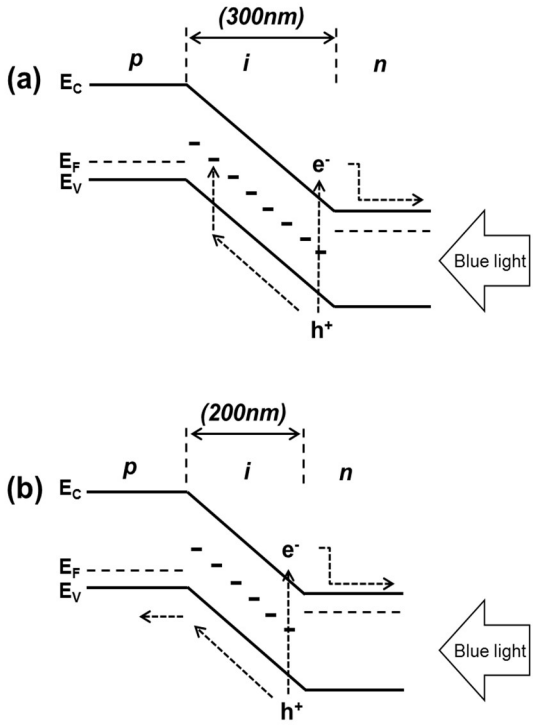

Figure 33. Possible carrier loss mechanism of negative biased photodiodes with (a) 300 and (b) 200 nm thick i-layer under blue light illumination.

5.5 Defect generation in intrinsic layer

In order to confirm the mechanisms described in the previous section, an a-Si:H pin diode with a 200nm-thick i-layer was intentionally stressed with a voltage under the light exposure condition. The goal was to show that defects generated in the i-layer could enhance the one-sided charge transfer phenomenon. Figure 34 shows J-V curves of the diode after (a) 0 min, (b) 5 min, and (c) 10min of the combined electric-light stress conditions, separately. Fig. 34(a) shows that before the stress, the J-V curves under all light illumination conditions were similar with those in Fig. 31(b). However, after 5 min of the combined electric-light stress, J-V curves changed the shape, especially under the blue and green light illuminations, obviously as shown in Fig. 34(b). After an additional 5 min stress, the shape of the J-V curves further deteriorated not only under the blue and green light illumination but under the red light illumination, as shown in Fig. 34(c). In addition, the current density of the diode decreased with the increase of the stress time under all light illumination conditions.

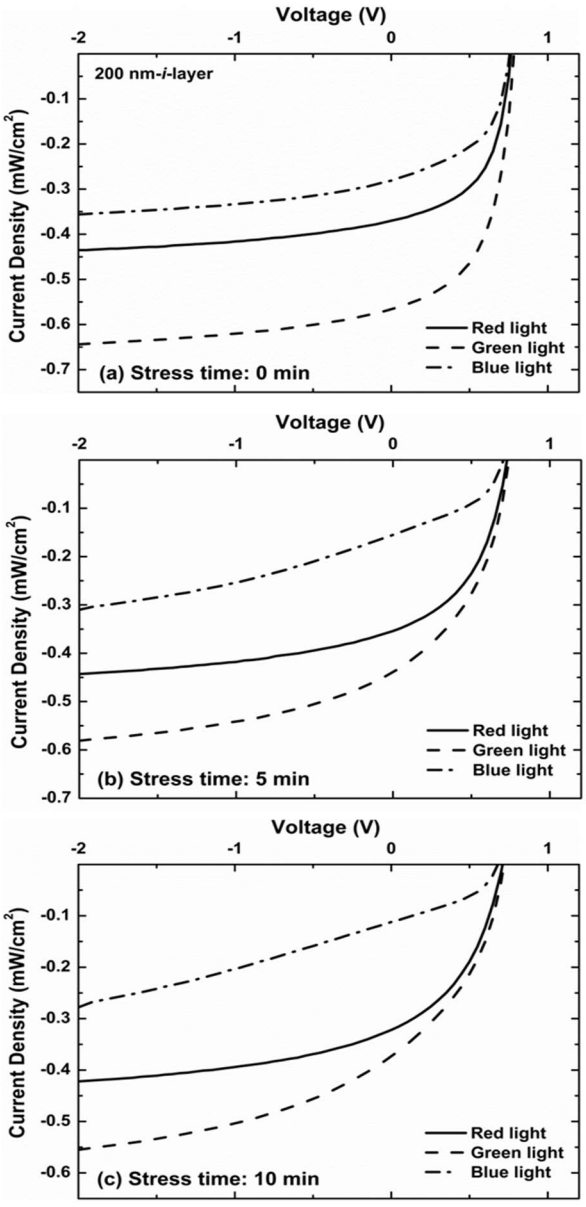

Figure 34. J-V characteristics of the same photodiode with 200nm i-layer after (a) 0, (b) 5, and (c) 10min of combined electric-light exposure stress.[91]

Figure 35 shows that changes of curves of the current density drop rate and EQE vs. wavelength of illumination light, which are calculated from Fig. 34. As the stress

time increases, the current density drop rate increases over all light illumination conditions. The current density drop rate decreases with the increase of the wavelength of the illumination light. For example, after 10 min stress, it increased by about 39, 21, and 9% under the blue, green, and red light illuminations, respectively. This trend is similar to that of Fig. 32. As discussed previously, the asymmetric loss of photo-generated holes and electrons was due to the long transfer path of the former through the i-layer. The thicker the i-layer was, the more the loss of holes was. Therefore, the total amount of defects in the i-layer is responsible for the availability of the measurable photocurrent. The combined voltage-light stress experimental result confirms the i-layer thickness effect.

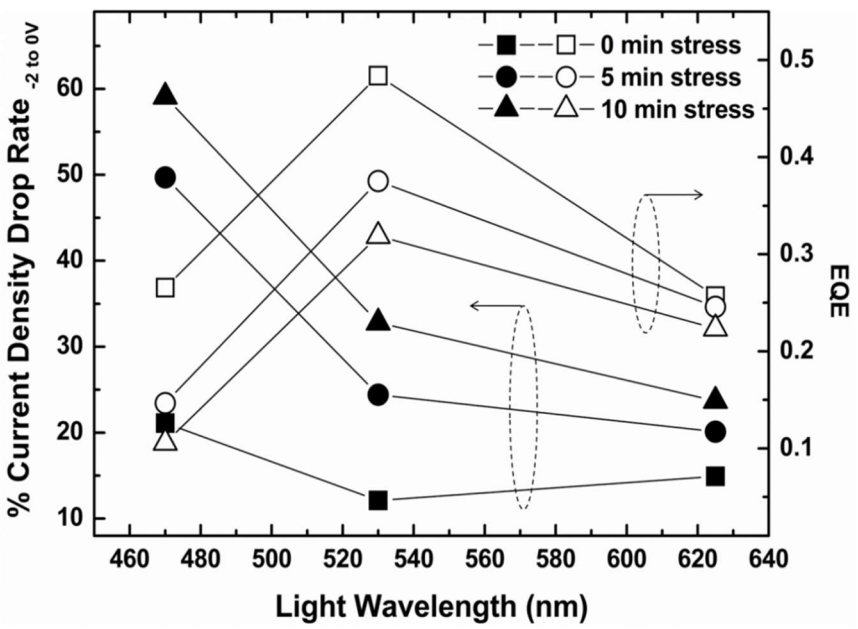

Figure 35. Changes of current density drop rate and EQE of the diode on combined stress under three different lights.[91]

5.6 Thickness vs. defect density effect under red light illumination

Figure 35 shows that the EQE changes with the wavelength of the illumination light under the voltage-light stress condition. The trend is similar to that in Fig. 32, except that in Fig. 35, the EQE change with the stress time is much smaller under the red light illumination condition than that with the i-layer thickness in Fig. 32. In Fig. 32, under the red light illumination, the EQE drops drastically with the increase of the i-layer thickness. The long wavelength red light can penetrate through the whole pin tri-layer without being totally absorbed.[90] Electrons and holes can be generated across the whole i-layer not limited to the i/n^+ interface.[8, 44] Therefore, the asymmetric loss of the photo-generated holes under the red light illumination condition is much less serious than that under blue or green light illumination. Consequently, the EQE was only a little reduced with the increase of the i-layer's defect density. In Fig. 32, though the thick i-layer is more favorable to the absorption of the red light than the thin i-layer, the EQE is inversely proportional to the i-layer thickness. Furthermore, the large improvement of the EQE under the red light illumination is attributed to the reduced i-layer in thickness, which may result from the increase of the carrier collection efficiency of the diode. Since the average traveling distance of the photo-generated electrons and holes across the i-layer is shorter in the thin i-layer than that in the thick i-layer, the carrier collection efficiency in the former is higher than that in the latter. Therefore, the light detection of the long wavelength light-illuminated diode is mainly contributed by the i-layer thickness.

5.7 Summary

The mechanism of the asymmetric carrier loss in the a-Si:H pin diode has been studied with the different i-layer thickness, combined voltage-light stress method, and three narrow band lights. Under all light illuminated conditions, the diode with the 200 nm-thick i-layer showed better electrical property than that with the 300nm-thick i-layer because in the former the asymmetric transfer phenomenon of photo-generated holes was minimized. This was confirmed from the combined voltage-light stress method. The property of the pin diode with the 200 nm-thick i-layer, which was stressed for a total of 10 min of the combined electric bias-light illumination condition, was very similar with that of the diode with the 300 nm-thick i-layer. In summary, the asymmetric carrier loss of the diode is affected by the i-layer thickness, the wavelength of the light, as well as the quality of the i-layer.

CHAPTER VI

CONCLUSIONS

In this dissertation, the light detection property of the solar cell and photodiode based on the a-Si:H pin diode has been studied with respect to external factors such as the film deposition sequence, light wavelength, light power density, and i-layer thickness.

The a-Si:H solar cells prepared in the single chamber PECVD suffer from the contamination of the i-layer caused by the dopant residue in the chamber left from the previous film deposition. The property of the i-layer is dependent on the film deposition sequence, which affects the cell performance, cell degradation, and the cell recovery. The pin structured diode showed better light detection than the nip structured diode. For the reliability and recovery tests, however, the opposite was true.

The light detection property of the a-Si:H pin diode has been investigated by controlling the power density of red (625nm), green (530nm), and blue (470nm) illumination lights. The poor response of the diode to the short wavelength illuminated light resulted from the one-sided loss of the photo-generated carriers because of the asymmetric traveling distance of the photo-generated electrons and holes. This phenomenon was more serious with the increase of the light power density.

The mechanism of asymmetric carrier loss of the a-Si:H pin diode has been discussed with regard to different i-layer thicknesses, combined electric-optical stress method, and three narrow-band lights. In Chapter IV, it was stated that the asymmetric light detection of the diode originated from the location of the photo-generated electron-

hole pairs in the i-layer, depending on the light wavelength. This result was demonstrated using the different i-layer thickness and combined electric-optical stress method.

REFERENCES

1. E. Fortunato, G. Lavareda, M. Vieira and R. Martins, *Rev. Sci. Instrum.*, 65, 3784 (1994).
2. D. Li, K. Kim, S. Zhang, G. Dong and Y. Kuo, *Sens. Actuators A: Phys.*, 236, 364 (2015).
3. C.-M. Hsu, C. Battaglia, C. Pahud, Z. Ruan, F.-J. Haug, S. Fan, C. Ballif and Y. Cui, *Adv. Energy Mater.*, 2, 628 (2012).
4. A. Becquerel, *Comptes Rendus*, 9, 561 (1839).
5. B. G. Streetman and S. j. Banerjee, *Solid State Electronic Devices*, Pearson Prentice Hall, Upper Saddle River, New Jersey (2006).
6. K. Masuko, M. Shigematsu, T. Hashiguchi, D. Fujishima, M. Kai, N. Yoshimura, T. Yamaguchi, Y. Ichihashi, T. Mishima, N. Matsubara, T. Yamanishi, T. Takahama, M. Taguchi, E. Maruyama and S. Okamoto, *IEEE Journal of Photovolt.*, 4, 1433 (2014).
7. J. Ohura, T. Tsukakoshi, K. Fukuda, M. Shimbo and H. Ohashi, *IEEE Electron Device Lett.*, 8, 454 (1987).
8. A. Shah, *Thin-Film Silicon Solar Cells*, EPFL press (2010).
9. R. M. Swanson, *Prog. Photovolt. Res. Appl.*, 14, 443 (2006).
10. K. L. Chopra, P. D. Paulson and V. Dutta, *Prog. Photovolt. Res. Appl.*, 12, 69 (2004).
11. Y. Kuo, *ECS Proceeding Thin Film Transistor Technologies IV*, p. 191 (1998).

12. S. Park, H. Yong Ji, M. Jun Kim, J. Hyeon Peck and K. Kim, *Appl. Phys. Lett.*, 104, 073902 (2014).
13. Y. Kuo, *Thin Film Transistor - Materials and processes Vol. 1: Amorphous Silicon Thin Film Transistor*, Kluwer Academic Publishers (2004).
14. D. L. Staebler and C. R. Wronski, *Appl. Phys. Lett.*, 31, 292 (1977).
15. R. Singh, S. Prakash, N. N. Shukla and R. Prasad, *Phys. Rev. B*, 70, 115213 (2004).
16. W. E. Spear and P. G. Le Comber, *Solid State Commun.*, 17, 1193 (1975).
17. W. E. Spear, *Adv. Phys.*, 26, 811 (1977).
18. R. A. Street, *Hydrogenated Amorphous Silicon*, Cambridge University Press (1991).
19. N. F. Mott, *Philos. Mag.*, 19, 835 (1969).
20. F. Urbach, *Phys. Rev.*, 92, 1324 (1953).
21. R. A. Street, *Appl. Phys. Lett.*, 59, 1084 (1991).
22. P. V. Santos, N. M. Johnson and R. A. Street, *Phys. Rev. Lett.*, 67, 2686 (1991).
23. W. B. Jackson and J. Kakalios, *Phys. Rev. B*, 37, 1020 (1988).
24. D. L. Staebler, R. S. Crandall and R. Williams, *Appl. Phys. Lett.*, 39, 733 (1981).
25. M. Riordan and L. Hoddeson, *IEEE Spectrum*, 34, 46 (1997).
26. S. M. Sze and K. K. Ng, *Physic of Semiconductor Devices*, John Wiley and Sons, Inc. (2012).
27. J. M. Boudry and L. E. Antonuk, *IEEE Trans. Nucl. Sci.*, 41, 703 (1994).
28. J. Kim, C. Battaglia, M. Charrière, A. Hong, W. Jung, H. Park, C. Ballif and D. Sadana, *Adv.Mater.*, 26, 4082 (2014).

29. K. Islam, A. Alnuaimi, E. Battal, A. K. Okyay and A. Nayfeh, *Sol. Energy*, 103, 263 (2014).
30. Y. Tawada, K. Tsuge, M. Kondo, H. Okamoto and Y. Hamakawa, *J. Appl. Phys.*, 53, 5273 (1982).
31. B. Chapman, *Glow Discharge Processes*, John Wiley, New York (1980).
32. J. L. Vossen and W. Kern, *Thin Film Process II*, Academic Press Inc. (1991).
33. Y. Kuo, Okajima, K. and Takeichi, M., *IBM J. Res. Dev.*, 43, 73 (1999).
34. A. Matsuda, *25th IEEE Photovoltaic Specialists Conference*, p. 1029 (1996).
35. A. Matsuda, M. Takai, T. Nishimoto and M. Kondo, *Sol. Energ. Mat. Sol. C.*, 78, 3 (2003).
36. K. Koga, N. Kaguchi, K. Bando, M. Shiratani and Y. Watanabe, *Rev. Sci. Instrum.*, 76, 113501 (2005).
37. J. Nelson, *The Physics of Solar Cells*, Imperial College Press (2003).
38. M. A. Green, *Solar Cells: Operating Principles, Technology and System Applications*, University of New South Wales (1982).
39. H. Mell and W. Beyer, *J. Non·Cryst. Solids*, 59–60, Part 1, 405 (1983).
40. N. M. Amer, A. Skumanich and W. B. Jackson, *J. Non·Cryst. Solids*, 59–60, Part 1, 409 (1983).
41. N. M. Amer, A. Skumanich and W. B. Jackson, *Physica B and C*, 117, 897 (1983).
42. Y. Uchida, M. Nishiura, H. Sakai and H. Haruki, *Sol. Cells*, 9, 3 (1983).
43. A. Dasgupta, N. Palit and S. Ray, *Sol. Energ. Mat. Sol. C.*, 55, 395 (1998).
44. S. C. Lee, *J. Appl. Phys.*, 55, 4426 (1984).

45. T. D. Moustakas, R. Friedman and B. R. Weinberger, *Appl. Phys. Lett.*, 40, 587 (1982).

46. M. K. Han, R. Lahri, W. A. Anderson and J. Coleman, *15 th IEEE Photovoltaic Spectialists Conference*, p. 685 (1981).

47. O. Cubero, F. J. Haug, Y. Ziegler, L. Sansonnens, P. Couty, D. Fischer and C. Ballif, *Sol. Energ. Mat. Sol. C.*, 95, 606 (2011).

48. T. Hitoshi, K. Makoto, L. Koeng Su, S. Porponth, K. Koichiro and T. Kiyoshi, *Jpn. J. Appl. Phys.*, 21, 219 (1982).

49. K. Kibum and K. Yue, *40th IEEE Photovoltaic Specialist Conference*, p. 3055 (2014).

50. H. Haruki, H. Sakai, M. Kamiyama and Y. Uchida, *Sol. Energ. Mat.*, 8, 441 (1983).

51. M. Foti, G. Cannella, C. Gerardi, S. Di Marco, S. Ravesi, N. Sparta, S. Lo Verso, F. Principato, S. Coffa and S. Lombardo, *Proceedings of the 220th ECS Meeting on Photovoltaics for the 21st Century*, p. 15 (2011).

52. G. Cannella, F. Principato, M. Foti, C. Gerardi and S. Lombardo, *Sol. Energy*, 88, 175 (2013).

53. G. G. Pethuraja, R. E. Welser, A. K. Sood, C. Lee, N. J. Alexander, H. Efstathiadis, P. Haldar and J. L. Harvey, *Adv. Mater. Phys. Chem.*, 2, 59 (2012).

54. M. Stutzmann, *Appl. Phys. Lett.*, 56, 2313 (1990).

55. H. R. Park, J. Z. Liu and S. Wagner, *Appl. Phys. Lett.*, 55, 2658 (1989).

56. S. R. Dhariwal and B. M. Deoraj, *J. Appl. Phys.*, 71, 4196 (1992).

57. T. Tiedje and A. Rose, *Solid State Commun.*, 37, 49 (1981).

58. Y. Kuo, *Appl. Phys. Lett.*, 61, 2790 (1992).

59. Y. Kuo, *Vacuum*, 59, 484 (2000).

60. A. Pandey, B. Cai, N. Podraza and D. A. Drabold, *Phys. Rev. Applied*, 2, 054005 (2014).

61. C. T. Sah, J. Y. C. Sun and J. J. T. Tzou, *Appl. Phys. Lett.*, 43, 204 (1983).

62. S. M. Pietruszko, M. Pachocki and J. Jang, *J. Non·Cryst. Solids*, 198–200, Part 1, 73 (1996).

63. N. Khelifati, S. Tata, A. Rahal, R. Cherfi, A. Fedala, M. Kechouane and T. Mohammed-Brahim, *Phys. Status Solidi (c)*, 7, 679 (2010).

64. J. Park, C. Shin, S. Lee, S. Kim, J. Jung, N. Balaji, V. A. Dao, Y.J. Lee and J. Yi, *Thin Solid Films*, 587, 132 (2015).

65. R. C. Chittick, J. H. Alexander and H. F. Sterling, *J. Electrochem. Soc.*, 116, 77 (1969).

66. R. A. Street, *Technology and Applications of Amorphous Silicon*, Springer (2013).

67. J. Chabbal, C. Chaussat, T. Ducourant, L. Fritsch, J. Michailos, V. Spinnler, G. Vieux, M. Arques, G. Hahm, M. Hoheisel, H. Horbaschek, R. F. Schulz and M. F. Spahn, *Medical Imaging 1996: Physics of Medical Imaging*, p. 499 (1996).

68. G. Dong, H. Zheng, L. Duan, L. Wang and Y. Qiu, *Adv.Mater.*, 21, 2501 (2009).

69. M. Ristova, Y. Kuo and H. H. Lee, *Appl. Surf. Sci.*, 218, 44 (2003).

70. M. Ristova, Y. Kuo and S. Lee, *Semicond. Sci. Technol.*, 18, 788 (2003).

71. D. Derkacs, S. H. Lim, P. Matheu, W. Mar and E. T. Yu, *Appl. Phys. Lett.*, 89, 093103 (2006).

72. R. R. Arya, A. Catalano and R. S. Oswald, *Appl. Phys. Lett.*, 49, 1089 (1986).

73. Y. Y. Cheng, B. Fuckel, R. W. MacQueen, T. Khoury, R. G. C. R. Clady, T. F. Schulze, N. J. Ekins-Daukes, M. J. Crossley, B. Stannowski, K. Lips and T. W. Schmidt, *Energy Environ. Sci.*, 5, 6953 (2012).

74. K. Seki, H. Yamamoto, A. Sasano and T. Tsukada, *J. Non·Cryst. Solids*, 59, 1179 (1983).

75. A. M. Pérez, C. Santiago, F. Renero and C. Zuñiga, *Optice*, 45, 123802 (2006).

76. X. Li, C. Zhang, Z. Yang and A. Shang, *Opt. Express*, 21, A677 (2013).

77. S. N. Agbo, T. Merdzhanova, U. Rau and O. Astakhov, *Sol. Energ. Mat. Sol. C.*, 159, 427 (2017).

78. C. T. Chu, P. D. Fuqua and J. D. Barrie, *Appl. Opt.*, 45, 1583 (2006).

79. S. Morawiec, M. J. Mendes, S. A. Filonovich, T. Mateus, S. Mirabella, H. Águas, I. Ferreira, F. Simone, E. Fortunato, R. Martins, F. Priolo and I. Crupi, *Opt. Express*, 22, A1059 (2014).

80. N. Sahraei, S. Venkataraj, A. G. Aberle and I. M. Peters, *Energy Procedia*, 33, 166 (2013).

81. J. Reichman, *Appl. Phys. Lett.*, 38, 251 (1981).

82. A. Rothwarf, *Appl. Phys. Lett.*, 40, 694 (1982).

83. R. B. Tagirov and L. P. Tagirov, *Russ. Phys. J.*, 40, 664 (1997).

84. P. Mialhe, J. P. Charles, A. Khoury and G. Bordure, *J. Phys. D: Appl. Phys.*, 19, 483 (1986).

85. M. A. Kroon and R. A. C. M. M. van Swaaij, *J. Appl. Phys.*, 90, 994 (2001).

86. P. Ashburn, D. V. Morgan and M. J. Howes, *Solid·State Electron.*, 18, 569 (1975).

87. A. S. Grove, *Physics and Technology of Semiconductor Devices*, Wiley (1967).

88. K. Kim and Y. Kuo, *ECS J. Solid State Sci. Technol.*, 6, Q29 (2017).

89. A. Klaver and R. A. C. M. M. van Swaaij, *Sol. Energ. Mat. Sol. C.*, 92, 50 (2008).

90. K. Kim and Y. Kuo, *ECS Trans.*, 72, 15 (2016).

91. K. Kim and Y. Kuo, *IEEE Sensors Lett.*, 1, ASN: 3500304 (2017): Reprinted, with permission, from © [2017] IEEE.

92. H. Wieczorek, *Solid State Phenom.*, 957, 44-46, (1995).

93. E. A. Schiff, *J. Phys. Condens. Matter*, 16, S5265 (2004).

94. E. A. Schiff, *Philos. Mag.*, 89, 2505 (2009).